Implementation of a dry surface layer soil resistance in two contrasting semi-arid sites with SURFEX-ISBA V9.0

Belén Martí[1], Jannis Groh[2,3,4], Guylaine Canut[1], and Aaron Boone[1]

[1]Météo-France, CNRS, Université de Toulouse, CNRM, Toulouse, France
[2]Institute of Crop Science and Resource Conservations (INRES), Soil Science and Soil Ecology, University of Bonn, Bonn, Germany
[3]Institute of Bio- and Geosciences - Agrosphere (IBG-3), Forschungszentrum Jülich GmbH, Jülich, Germany
[4]Research Area 1 Landscape Functioning, Isotope Biogeochemistry and Gas Fluxes, Leibniz Centre for Agricultural Landscape Research (ZALF), Müncheberg, Germany

Correspondence: Belén Martí (belen.marti@meteo.fr)

Abstract. The estimation of latent heat fluxes in semi-arid regions faces several challenges, such as human intervention in the water cycle through irrigation, sudden changes in vegetation state due to crop harvesting, the still evolving knowledge of the physical processes governing plant transpiration and soil evaporation, and the lack of measurements to develop and test land surface models. Representing the wide range of evapotranspiration values presents difficulties for both simulations
5 and measurements, owing to strong soil/plant spatial heterogeneity at relatively small (e.g. hectometric) scales. The ability to accurately predict the partition of evapotranspiration into evaporation and transpiration from observation is still very limited, but improved estimates are required so that better water use decisions can be made. Land surface models (LSMs) can be used as a tool in this regard, when their validation is possible, simulations tend to overestimate soil evaporation in most models.

The simulations in this study make use of the LSM ISBA, which represents the land component within the surface coupling
10 platform SURFEX. They include two field sites with contrasting soil moisture and vegetation characteristics during the summer of the Land surface interactions with the atmosphere over the Iberian semi-arid environment (LIAISE) campaign. The first site corresponds to a full cutting and growing cycle of one month in a flood irrigated alfalfa field. A detailed examination of the parametrization suggests that several parameters determine the amount and tendency of transpiration change. ~~In particular, a higher quantum efficiency and maximum assimilation are marked as the driving model parameters together with a mesophylic~~
15 ~~conductance value closer to C4 behavior.~~ The second site is an uncultivated rain-fed area of natural grass close to senescence. As the parametrization of the vegetation proved to be insufficient to characterize the evapotranspiration, for this study the implementation of a dry surface layer (DSL) resistance within the LSM ISBA was developed. The consideration of this process characterizes the transfer of vapor in a physical way that has proved successful in improving the partitioning of evapotranspiration in other models. The implementation of a DSL resistance led to an improvement in the simulated latent heat
20 flux by reducing bare soil evaporation compared to simulations without a soil resistance. This approach resulted in a reduction in daily latent heat flux RMSE of 29% and 32% for the alfalfa and natural grass site respectively, while increasing slightly the correlation by 0.02 and 0.01 at both sites. Sensible heat flux and net radiation are improved on the order of $10\,\mathrm{W\,m^{-2}}$ whereas the ground heat flux is deteriorated within the same order. The resulting DSL simulations reduced the overall global error

compared to a simulation without a DSL resistance. Sensitivity tests of the parameters that drive a DSL resistance in ISBA further improve the simulations, reducing excessive damping after rain events. The new DSL parameterization helps overcome current problems of ET modelling by reducing bare soil evaporation within LSMs.

Short Summary. The characterization of vegetation at two sites proved insufficient to simulate adequately the evapotranspiration. A dry surface layer was implemented in the land surface model SURFEX-ISBA v9.0. It is compared to simulations without a soil resistance. The application to an alfalfa site and a natural grass site in semiarid conditions results in an improvement in the estimation of the latent heat flux. The surface energy budget and the soil and vegetation characteristics are explored in detail.

1

Semi-arid environments are characterized by water deficits during part of the year. In these areas, water resource management is essential for food production and water use for the local population, as water scarcity is common. In particular, the estimation of water loss by evapotranspiration (ET) is a challenge in these areas due to several factors, such as the significant heterogeneity of land surface characteristics, low values of fluxes at the limits of observational capabilities (Mauder et al. 2020), anthropic changes in land use such as the harvesting of crops and in land management such as irrigation, and complex underrepresented processes in the unsaturated zone of the soil (e.g. secondary drying fronts, pore scale influence such as in Or et al. 2013). As a result, such processes are still being studied and incorporated to the models. Global estimates of ET reveal seasonal differences depending on the product (Jiménez et al. 2011) and the method (Coenders-Gerrits et al. 2014; Schlesinger and Jasechko 2014). The transpiration ratio, the proportion of water vapor released through transpiration relative to total ET, is critical in assessing the potential improvement of water use through the regulation of transpiration (Yoo et al. 2009). Estimates of the ratio range from transpiration-dominated (Miralles et al. 2011) to evaporation-dominated (Alton et al. 2009) ecosystems when estimated from satellite and model-derived ET. The observed range of transpiration ratios, from 38% to 77%, can largely be attributed to differences in leaf area index (LAI) estimates across the reviewed studies (Wang et al. 2014). Since LSMs tend to have a low transpiration ratio (Chang et al. 2018) and tend to overestimate the evaporative fraction and the bare soil evaporation after rain events (Lohou et al. 2014), a better representation of soil resistances can serve to improve the soil evaporation in the models, leading to better partitioning of ET and a reduction in near surface temperature biases in atmospheric models (Dong et al. 2020).

LSMs estimate ET and its partitioning with varying complexity (Noilhan and Planton 1989; Sellers et al. 1996; Coudert et al. 2006; Napoly et al. 2017). ET estimates can be made without distinguishing between sources, as in the Priestley-Taylor or Penman-Monteith methods, or by partitioning ET into bare soil evaporation, transpiration and evaporation from the interception of residual water on the leaves using similarity theory. Transpiration is modeled using a resistance analogue ~~, with a canopy resistance which represents plant biophysical processeswhich can include the~~ together with the humidity gradient. The resistance represents the canopy biophysical processes. One of the configurations includes the assimilation of carbon, ~~the~~

2

~~latter allows to modify the parameters to a particular plant species~~which allows the specification of species-dependent plant parameters.

Bare soil evaporation in the unsaturated zone is characterized by the simultaneous presence of water in both liquid and vapor phases within the soil. Explicit treatment of soil water vapor requires full coupling between the transfer of heat and the transport of water (Philip and De Vries 1957; Milly 1984), which is very sensitive to soil hydraulic properties (Chanzy et al. 2008; Merlin et al. 2016). They can modify the behavior of capillary continuity and exchange processes from pores through air to the atmosphere, determining transport processes across soil drying stages (Or et al. 2013). Up to four stages of drying soil can be identified (Zhang et al. 2015): ~~a first~~ 1) stage of ponding, 2) a period of air intrusion into the soil, 3) a rapid drying until no liquid remains and, 4) a residual layer drying as the vaporization plane descends and a dry surface layer (DSL) forms (Balugani et al. 2018). A more common approach is to separate soil evaporation in two stages. Stage 1 depends mostly on the atmospheric energy demand and drives a constant rate of evaporation. Stage 2 evaporation is controlled by the soil characteristics. The rate of evaporation depends on the type of soil and its soil hydraulic properties (Schneider et al. 2021). The implicit treatment of bare soil evaporation can be modeled by a soil resistance thereby simplifying the coupling that depends on radiation, liquid water gradients and temperature gradients to a dependence on water content, and in some cases, also on the temperature.

~~Several empirical soil resistance approaches have been developed since the nineties~~Such empirically-based soil resistances have been used for years in various land surface models (Sellers et al. 1992b; Best et al. 2011; Harris et al. 2017; Raoult et al. 2018), as simulated latent heat fluxes (especially from the soil) were found to be overestimated in their ~~model (Sellers et al. 1992b), and more recently~~more physically meaningful resistances have been parameterized (Swenson and Lawrence 2014) (see more respective models. The tuned values of these resistances can have a large impact on the water balance components in addition to the evaporation, such as for the runoff (Cuntz et al. 2016).

More recently, models have applied more data-driven approaches (Merlin et al. 2016; Lehmann et al. 2018; Raoult et al. 2021) to constrain case-dependent results and physically based resistances (Sakaguchi and Zeng 2009; Zhang et al. 2015; Swenson and Lawrence as knowledge of soil physics advances. These resistances differ in the value of the volumetric water content (VWC) at which they become active, whether its form is exponential or linear, and in terms of the magnitude of the resistance. Two resistances are of particular interest, the first by Sellers et al. (1992b) due to its longstanding wide use, and the second by Swenson and Lawrence (2014) which is based upon a more physically meaningful resistance with larger values (more details are provided in Sect. 2.2.1). The aforementioned study used the FLUXNET dataset (Jung et al. 2009) and a model tree ensemble approach to analyze behavior on a global scale. By implementing the DSL in the Interactions Soil-Biosphere-Atmosphere (ISBA) model (see Sect. 2), we investigate whether it can improve its estimation of bare soil evaporation and consequently ET.

Both the Sellers et al. (1992b) and the Swenson and Lawrence (2014) parametrizations are tested in detail for two sites that were operated during the *Land surface interactions with the atmosphere over the Iberian Semi-arid environment* (LIAISE) campaign, described in Sect. 3.1. They represent the extremes found in the semi-arid environment in terms of Bowen ratio: the first site is a flood irrigated alfalfa field where ET dominates, and the second is an almost senescent rainfed natural grass site where sensible heat flux dominates. Together these two sites provide a good test case for studying the limits of the model and for evaluating the default and new parametrizations with a DSL.

2 Model description

ISBA includes a Multi-Energy Budget (MEB) model option described in Boone et al. (2017) which uses a classical Big-Leaf type approach ~~to modeling the SEB~~for modeling the surface energy budget (SEB). MEB separates ~~ET~~ latent heat flux (LE) as the contribution of soil evaporation, transpiration, interception of evaporation and sublimation when snow is present. It allows separate consideration of vegetation-driven processes, such as the impact of stomatal conductance and light assimilation on transpiration, and of soil processes, such as soil evaporation and the impacts of a litter layer. MEB can also represent vertical heterogeneity of the soil hydraulic and thermal properties across the soil profile. ISBA-MEB within SURFEX (*Surface Externalisée*: Externalized Surface) version V9 is used in this article together with the multilayer diffusive soil scheme option (Decharme et al. 2011). To date, the local scale evaluation of ISBA-MEB has been carried out with trees (Napoly et al. 2017), corn (Dare-Idowu et al. 2021) and in a semi-arid environment in a vineyard (Aouade et al. 2020).

2.1 Components of the latent heat flux

The ~~latent heat flux (LE)~~ LE can be found by the evaporative contribution of the vegetation and the soil:

$$LE = L_v \left(E_v + E_g \right) \tag{1}$$

where L_v is the latent heat of evaporation and E_g is the part of the flux originated from soil evaporation ~~. It is described in detail subsection 2.2~~(see subsection 2.2). E_v is given by the sum of the plant transpiration E_{tr} and the evaporation from the canopy liquid water interception store E_r, when no snow is present. ~~They are given by:~~

~~$$E_{tr} = \rho_a \frac{q_{sat,v} - q_c}{R_{avg-c} + R_s} (1 - \delta)$$~~

~~and~~

~~$$E_r = \rho_a \frac{q_{sat,v} - q_c}{R_{avg-c}} \delta$$~~

~~with $R_s = 1/g_{sI}$ where g_{sI} is the stomatal conductance at the canopy level and it is the weighted average of the different plant types multiplied by the LAI, ρ_a is the air density, $q_{sat,v}$ is the saturated specific content at the vegetation temperature and q_c is the canopy air specific humidity ($kgkg^{-1}$). R_{avg-c} is the resistance between the overlaying air and vegetation. It consists on the inverse of the sum of the bulk canopy aerodynamic conductance between the canopy and the canopy air (Choudhury and Monteith 1988) and the conductance accounting for the free convection from (Sellers et al. 1986). δ is the Halstead coefficient with a factor to account that saturated vegetation can transpire. See Boone et al. (2017) section 2.6.1 for the particulars of the aerodynamic resistance of the canopy, section 2.8.3 for the Halstead coefficient and their appendix C2 for the LE formulation, which fall outside the discussions of this article.~~

2.2 ~~Transpiration formulation: A-gs~~

The A-gs (Assimilation-stomatal conductance) scheme of Goudriaan et al. (1985) within SURFEX presents the parametrization of plant assimilation of carbon. It was modified by Jacobs et al. (1996) to model photosynthesis and it can be used to obtain transpiration. Different types of vegetation can be selected and its parametrizations are modeled as a function of the so-called vegetation patch (or land cover type). In SURFEX, a patch corresponds to a Plant Functional type (PFT), which characterizes subcategories natural land-surfaces. Additionally, vegetation can have either drought tolerant or drought avoidant strategies (Calvet et al. 2004). A description of the processes can be found in Calvet et al. (1998) and Delire et al. (2020).

In order to discuss the parameter selection, we provide the mathematical development of the low vegetation scheme in ISBA (Calvet 2000), which is used to represent crops. Transpiration in A-gs is given by:

$$E_T = \rho_a g_s D_s$$

D_s is the specific humidity deficit. D_s indicates when stomata are closed by exceeding D_{max}, the maximum specific humidity deficit of the air tolerated by the vegetation (with no soil water stress). D_s is of the form:

$$D_s = \frac{f - f_0^*}{f_{min} - f_0^*} D_{max}$$

where f indicates the proportionality of internal CO_2 and inside the leaf boundary layer and f_0^* is f with no saturation deficit (without soil water stress) and are model parameters (see Table A1). f_{min} is the minimal value of f:

$$f_{min} = \frac{g_c}{g_c + g_m^*}$$

where g_m^* is the mesophyllic conductance and g_c is the cuticular conductance. g_m^* determines the gas exchange amount through the stomata and g_c through the cuticle when stomata are completely closed. The cuticle is a kind of wax membrane that protects the leaf and allows little exchange of gases, its values being smaller than those of g_m^*. Both contribute to the total transpiration.

Table of default parametrized values in the A-gs scheme for the used PFT.

	f	f_0^*	D_{max}^N	D_{max}^X	f_{2c}	$Q_{10}(25)$	$T_1(g_m^*, A_{m,max})$	$T_2(g_m^*, A_{m,max})$
units	m^2 kg^{-1}	-	g kg^{-1}	g kg^{-1}	-	-	$^\circ C$	$^\circ C$
C3 herbaceous	6.73	0.25	30	300	0.3	2.0	5,13	36,36
C4 crop	-4.33	0.15	30	300	0.3	2.0	8,13	38,38

2.1.1 Evaporation strategies

D_{max} behavior varies with evaporation strategy, limiting transpiration depending on its value. The formulation is the following:

$$D_{max} = D_{max}^+ + (D_{max}^* - D_{max}^+)\frac{f_2 - f_{2c}}{1 - f_{2c}}$$

where D_{max}^+ can be N for the drought-avoiding strategy applied for C3 crops, and X for the drought-tolerant strategy. For C3 crops D_{max}^* is given by:

$$\ln(g_m^*) = 2.381 - 0.6103 \ln(D_{max}^*)$$

and

$$f_2 = \sum_{i=1}^{Ng} \zeta_i \frac{\omega_{g,i} - \omega_{wilt,i}}{\omega_{fc,i} - \omega_{wilt,i}}$$

where f_2 is the normalized soil moisture and f_{2c} is its tabulated critical value. f_2 is summed over the soil layers Ng (Decharme et al. 2011) . Soil water content variables are represented by ω. The first subindex indicates the water content variable, g is the ground, $wilt$ is the wilting point and fc is the field capacity. The second subindex corresponds to the layer number to which it pertains, 1 would indicate the most superficial layer. ζ_i represents the difference in the cumulative root zone fraction for a given layer. Within this strategy D_{max} increases until critical soil moisture is reached ($f_2 = f_{2c}$), then the previous g_m^* symbolized by g_m^{*X} is updated and decreases with the water deficit: $g_m^* = g_m^{*X} f_2 / f_{2c}$.

For the drought tolerant strategy used for C4 crops and in our simulated alfalfa, we take Eq. (A6), with D_{max}^* given by:

$$\ln(g_m^*) = 5.323 - 0.8923 \ln(D_{max}^*)$$

In this strategy then D_{max} increases until the critical soil moisture is reached, D_{max} decreases with the severity of the stress: $D_{max} = D_{max}^X f_2 / f_{2c}$. Note that this is the opposite behavior as D_{max} and g_m^* are anticorrelated.

2.1.1 Stomatal conductance

To obtain g_s we use the following expressions:

$$g_s = 1.6 g_{sc} + g_c$$

where g_{sc} is the stomatal conductance to CO_2 given by:

$$g_{sc} = g_{sc}^{first} + E^{first} \frac{M_a}{\rho_a M_v} \frac{C_s + C_i}{2(C_s - C_i)}$$

where M_a and M_v are molecular masses of air and water vapor respectively, C_s is the external concentration of CO_2 and C_i The description for the vegetation description of the model can be found in the CO_2 internal concentration, expressed as:

$$C_i = f C_s + (1 + f) \Gamma$$

and

$$\Gamma(Ts) = \Gamma(25) Q_{10}^{Ts - 25} / 10$$

where Γ is the CO_2 compensation concentration at the skin temperature, Ts is the superficial temperature of the leaf and Q_{10} is fixed at 2.0 (see Table A1). Appendix A with a glossary in Appendix D. For completion, the G flux is also described in Appendix C1.

To obtain E^{first} with equation (A3), $g_s^{first} = 1.6 g_{sc}^{first}$ accounting for the ratio of CO_2 to water assimilation for the stomatal conductance to CO_2 with:

$$g_{sc}^{first} = \frac{A_n - A_{min} \left[\frac{D_s}{D_{max}^*} \left(\frac{A_n + R_d}{A_m + R_d} \right) + R_d \left(1 - \frac{A_n + R_d}{A_m + Rd} \right) \right]}{C_s - Ci}$$

where $R_d = A_m/9$ and corresponds to the dark respiration. A_m is the CO_2 assimilation limited by the air CO_2 concentration due to saturation, and A_n is the CO_2 assimilation limited by the air CO_2 concentration. A_{min} represents the residual photosynthesis rate (at full light intensity) associated with cuticular transfers when the stomata are closed because of a high specific humidity deficit, it is expressed as:

$$A_{min} = g_m^*(C_{min} - \Gamma)$$

where C_{min} is the minimum value of C_i at D_{max}^*, given by:

$$C_{min} = \frac{g_c C_s + g_m^* \Gamma}{g_c + g_m^*}$$

Additionally, A_m is:

$$A_m = A_{m,max}\left(1 - \exp\frac{-g_m^*(C_i - \Gamma)}{A_{m,max}}\right)$$

with:

$$A_{m,max} = \frac{A_{m,max}(25) Q_{10}^{(T_s - 25)/10}}{(1 + \exp\left[0.3(T_1 - T_s)\right])(1 + \exp\left[0.3(T_s - T_2)\right])}$$

with T_1 and T_2 being reference values.

$$A_n = (A_m + R_d)\left(1 - \exp\left(\frac{-\epsilon I_a}{A_m + R_d}\right)\right) - R_d$$

where

$$\epsilon = \epsilon_0 \left(\frac{C_i - \Gamma}{C_i + 2\Gamma}\right)$$

where ϵ_0 is the quantum efficiency.

The relationships from (A3) to (A20) show that g_s is highly nonlinear with the parameters g_m^*, g_c, A_{max} and ϵ_0. D_s is in fact $D_s(g_m^*, g_c)$ and $A_n = A_n(g_m^*, g_c, \epsilon_0, A_{max})$ between others. Discussion on the values of these parameters is done in Sect. 4.2.1.

2.2 Bare soil model formulation

The SURFEX V9 MEB bare soil evaporation with soil resistance consists in a mixed form soil resistance such as in Niu et al. (2011), Xue et al. (1996) and Sellers et al. (1996). A mixed formulation consists in adding a soil resistance (beta type formulation) to the aerodynamic resistance while also using a soil humidity factor applied to the saturated specific humidity in the numerator (alpha type formulation). This added mixed formulation is incorporated in the ground evaporation expression as:

$$E_g = \rho_a \left(\frac{h_u q_{sat,g} - q_c}{R_{ag} + R_{soil}}\right) \tag{2}$$

R_{ag} is the air resistance (s m^{-1}), R_{soil} is the soil resistance, q_{satg} is the saturated specific humidity of the air calculated with temperature of the ground at its first layer and h_u is the soil humidity coefficient which has the form:

$$h_u = \begin{cases} \frac{1}{2}\left[1 - \cos\left(\frac{w_{g,1}}{w_{fc,1}}\right)\right], & w_{g,1} < w_{fc,1} \\ 1, & w_{g,1} \geq w_{fc,1} \end{cases} \tag{3}$$

and when $h_u * q_{satg} < q_c$ and $q_{satg} > q_c$ then either there's no soil evaporation because the low level humidity is dry (~~$Eg = 0$~~ $E_g = 0$) or $h_u * q_{satg} < q_c$ and $q_{satg} \leq q_c$ which implies condensation (Noilhan and Mahfouf 1996). The default version of ISBA only included the humidity factor, h_u (and thus was uniquely an alpha formulation).

2.2.1 Soil resistances

~~Overestimation of~~ The overestimation of ET in land surface models is a lingering issue (Lohou et al. 2014). In particular, it has been shown that bare soil evaporation is generally ~~present~~ overestimated in LSMs (Chang et al. 2018), leading to overestimation of global ET (Wang et al. 2021). ~~The~~ In addition, the partitioning of ET into transpiration and soil evaporation is the main source of inter-model differences ~~for simulated ET amongst~~ among different models (Feng et al. 2023). ~~Empirically-based soil resistances have been used for years in various models (Takata et al. 2003; Best et al. 2011; Harris et al. 2017; Raoult et al. 2018) with tuned values that can have a large impact on water balance components, such as runoff (Cuntz et al. 2016).~~

Several forms of soil resistance have been proposed over the years ~~(Barton 1979; De Silans et al. 1989; Sellers et al. 1992b; Van de Grien~~ (Barton 1979; De Silans et al. 1989; Sellers et al. 1992b; Van de Griend and Owe 1994; Xue et al. 1996; Camillo and Gurney 1986; Moha , some of which have been tested within ISBA (Béziat et al. 2013). ~~These~~ The early citations were based on identifiable changes in the soil~~.~~, while satellite information has been added in more recent years.

De Silans et al. (1989) reported that the influence of soil resistance on evaporation was significant and goes along with a change in soil color together with a change in albedo measurements. Van de Griend and Owe (1994) observed the superficial DSL color change to a soil depth of 2.5 cm, together with a lower volumetric water content compared to the underlying layer and an increased estimation of the soil resistance value.

~~More recently, models have applied more data-driven approaches (Merlin et al. 2016; Lehmann et al. 2018; Raoult et al. 2021) to constrain case-dependent results and physically based resistances (Sakaguchi and Zeng 2009; Zhang et al. 2015; Swenson and Lawrence as knowledge of soil physics advances. These resistances differ in the value of the volumetric water content (VWC) at which they become active, whether its form is exponential or linear, and in terms of the magnitude of~~ The soil drying process of the DSL has been explored in laboratory conditions (Or et al. 2013; Zhang et al. 2015; Wang 2015; Merz et al. 2016; Balugani et al. 2021) . The results of these studies have led to a better understanding of the ~~resistance.~~ DSL formation process, and its impact on ET. Other processes, such as corner and film flow, are being explored in other communities and allow the identification of soil hydraulic properties with models such as HYDRUS in medium to dry conditions (Iden et al. 2021), but this level of sophistication fall outside the scope of this article.

The formulations cited here all produce lower resistance values than Sellers et al. (1992a) except for the DSL resistance as implemented by Swenson and Lawrence (2014). A comparison of resistance values for several standard soil resistance

formulations over a range of soil water contents is shown in Fig. 6 of Swenson and Lawrence (2014), which shows that the
235 DSL approach has the largest values. The DSL resistance was tested successfully globally in Swenson and Lawrence (2014).
In the current study, we investigate this method in detail using the LIAISE data.

~~The soil drying process has been explored in laboratory conditions (Or et al. 2013; Zhang et al. 2015; Wang 2015; Merz et al. 2016; Balu~~
~~. The results of these studies have led to a better understanding of the process of DSL formation and its impact on ET.~~
~~(Iden et al. 2021) has shown that including processes such as corner and film flow allows the identification of soil hydraulic~~
240 ~~properties with models such as HYDRUS in medium to dry conditions.~~

2.2.2 Sellers, 92

A widely ~~available expression among LSMs such as~~ used expression for soil resistance among LSMs, such as the community
Noah-MP (He et al. 2023), PX LSM WRF/CMAQ (Ran et al. 2016), ISBA-MEB (Boone et al. 2017), ORCHIDEE (MacBean
et al. 2020) ~~for the soil resistance~~ originated from Sellers et al. (1992b, 1996) and is formulated as:

$$245 \quad R_{soil} = \exp\left[A - B\left(\frac{w_{g,1}}{w_{sat,1}}\right)\right] \tag{4}$$

where A=8.206 and B=4.255 (Sellers et al. 1992b). These values were computed using field measurements taken during the
FIFE 89 campaign in Kansas (Sellers et al. 1992a) by inverting the SiB model (Sellers et al. 1992b) and finding the best fit for
several sites in the area.

2.2.3 Dry soil layer resistance

250 A DSL resistance is tested in SURFEX as an alternative for a soil resistance to Sellers 92. It models sites where compaction
and very intense heat cause all liquid water to be lost in the first few centimeters. This results in the formation of a DSL
that makes evaporation difficult: this impediment to evaporation is due to the transport of water being done only by vapor
water diffusion. This process is modeled in a pragmatic manner by using a surface layer resistance. According to Swenson and
Lawrence (2014), a DSL can be parameterized by the equation:

$$255 \quad \Delta DSL = \begin{cases} \Delta z_{dsl} \left(w_{dsl0} - w_{g,1}\right) / \left(w_{dsl0} - w_{air}\right), & w_{g,1} < w_{dsl0} \\ 0, & w_{g,1} \geq w_{dsl0} \end{cases} \tag{5}$$

where Δz_{dsl} is the length scale of the maximum ΔDSL thickness (m) and is given a value of 0.015 m as in Swenson and
Lawrence (2014), and w_{dsl0} is the moisture value at which the DSL becomes active. w_{dsl0} depends on the porosity (Φ) from
$w_{dsl0} = K_{dsl}\Phi$ where $K_{dsl} = 0.8$ is the value found by Swenson and Lawrence (2014) which improves their ET estimation
in semi-arid conditions. The porosity is defined as the saturated volumetric water content ($w_{sat,1}$) of the first layer, as this
260 corresponds to the pore space available for water. $w_{g,1}$ corresponds to the moisture value at the top soil layer of the model,
while w_{air} is the "air dry" soil moisture defined as

$$w_{air} = w_{sat,1}\left(\frac{\Psi_{sat}}{\Psi_{air}}\right)^{1/b} \tag{6}$$

where the air dry matric potential is $\Psi_{air} = -10^4$ m, the saturated matric potential is represented by Ψ_{sat} and the slope of the soil water retention curve is b. The soil resistance is expressed as

$$R_{soil} = \frac{\Delta DSL}{D_{\nu a}\tau_v} \tag{7}$$

where τ_v is the tortuosity of the vapor flow paths through the soil matrix and $D_{\nu a}$ is the molecular diffusivity of water vapor flow in air (m^2 s^{-1}). The expression of $D_{\nu a}$ differs slightly from that used in Swenson and Lawrence (2014) through the dependence on pressure, p, and the exponent of temperature:

$$D_{\nu a} = 2.17 * 10^{-5} \left(\frac{p_0}{p}\right)\left(\frac{T_{g,1}}{T_f}\right)^{1.88} \tag{8}$$

where p_0 is a standard reference pressure (1000 hPa), $T_{g,1}$ being the first level of soil temperature and T_f is the freezing temperature of water.

The tortuosity is then given by:

$$\tau_v = \Phi_{air}^2 \left(\frac{\Phi_{air}}{\Phi}\right)^{3/b} \tag{9}$$

where $\Phi_{air} = \Phi - w_{air}$ and represents the air-filled pore space.

3 Data and sites

3.1 The LIAISE campaign

The LIAISE campaign (Boone et al. 2025) was designed to improve the understanding of the impact of anthropization on the water cycle in semi-arid environments, with a particular focus on identifying the limitations of LSMs under these conditions. The field experiment took place in the north-eastern region of the Iberian Peninsula from April 2021 to the end of September 2021 (the Long Observational Period, LOP). Surface energy budget stations were installed over alfalfa (Canut 2022a; Mangan et al. 2022), maize (Martínez-Villagrasa et al. 2022), irrigated grass (Miró 2021), vineyard, apple orchard, almond orchard (Canut 2022b) and natural rainfed grass (Price 2023). They consisted in eddy-covariance systems equipped with a gas analyser to measure the turbulent fluxes and buried sensors including buried temperature sensors and flux plates, allowing the measurement of the ground flux directly and correction of its measurement to the surface (see Table E1) with the calorimetric method (de Silans et al. 1997). An intensive Special Observation Period (SOP) took place during July 15-29 (Boone et al. 2025), with in-situ measurements of soil and vegetation properties and of the atmospheric boundary layer (ABL) up to the entrainment zone through a multi-institutional collaboration (Brooke et al. 2023). The region is characterized by an irrigated area with fruit trees, maize and alfalfa, and a rainfed area with wheat, olives, almonds and natural grassland. The two areas are separated by the Canal d'Urgell. This configuration creates a profound contrast in the SEB components between the areas. The two main sites of the campaign, La Cendrosa and Els Plans, included a 50 m tower, SEB station and meteorological measurements, radio soundings, LAI and vegetation height observations (Boone et al. 2025).

Two surface stations were installed at la Cendrosa, the longer series was taken (Canut 2022a). Measurements of temperature, humidity and wind at different levels depending on sensor availability and high frequency measurements were available 3 m, 10 m, 25 m and 50 m for the two sites (see Boone et al. (2025) and Brooke et al. (2023) for more details).

3.2 Irrigated alfalfa site: La Cendrosa

The La Cendrosa site is located within an alfalfa field that was irrigated by gravity flooding approximately every ten days during the growing season and periodically cut for harvest. A cycle of cutting and growing during the month of July 2021, characterized by in-situ values of LAI and vegetation height, is prescribed as input (Fig. 1) for ISBA. The period starts with fully grown vegetation, but after a few days, the vegetation is cut. Growth starts rapidly after the next irrigation period and the vegetation height increases from about 10 cm to its maximum height of approximately 70 cm in 17 days. The LAI increases accordingly (from 0.3 to 3) over the same period.

This rapid vegetation evolution has an impact on the observed fluxes (Fig. 2). Initially, the net radiation (Rn) starts at values near 680 W m^{-2} and decreases a few days after mowing. However, the change is not immediately apparent in the measurements as it takes several days for the harvested alfalfa to be removed from the soil as it is left to dry in the field. After the initial growth period, when LAI is sufficient to cover most of the soil, the Rn returns to values close to 600 W m^{-2}. These observed values are not as high as before harvest because the water content is lower than after irrigation and this results in a higher albedo (see Sect. 5.3). LE is the dominant flux at this site, and the ground heat flux (G) and the sensible heat flux (H) represent a small part of the energy balance, except for the period after cutting and at the beginning of the growing period. The energy balance residue (Res) can be 100 W m^{-2} and negative during the day. It is defined as the residual available energy remaining after the Rn has been redistributed in the atmospheric and ground heat fluxes. The highest values of the residual are observed during periods of high vegetation. When vegetation is low, the value of the residue remains low or negative.

3.3 Dry rainfed natural grass site: Els Plans

The Els Plans site is a rainfed, relatively dry area with natural grass that was drying during the LOP. The parcel is located within a special protection area for steppe birds, and it is not cultivated. The energy budget of a short dry-down period near the end of the LOP (Fig. 3) shows a lower Rn compared to La Cendrosa ~~, because the~~ with two small rain contributions of 2 mm and 0.8 mm on the eve of 2 September. The Rn difference is due to the contribution of the net long wavelength radiation ~~is~~ being lower and the ~~soil albedo is lower~~ time difference between the two periods which can account up to 100 W m^{-2}. The small amount of water available in the soil makes the H the dominant term to compensate the Rn. The G can reach values twice as high as the LE, except after rain events, when the evaporation from the bare ground peaks. The energy budget residual at this site tends to be greater in the early morning, and it is reduced after the entry of the Marinada, a local sea breeze wind (Jiménez et al. 2023). This behavior is also observed in La Cendrosa when the vegetation is low. As a colder wind (Lunel et al. 2024), the Marinada advects moisture and cool air, and contributes negatively to the energy budget, bringing the residue closer to zero.
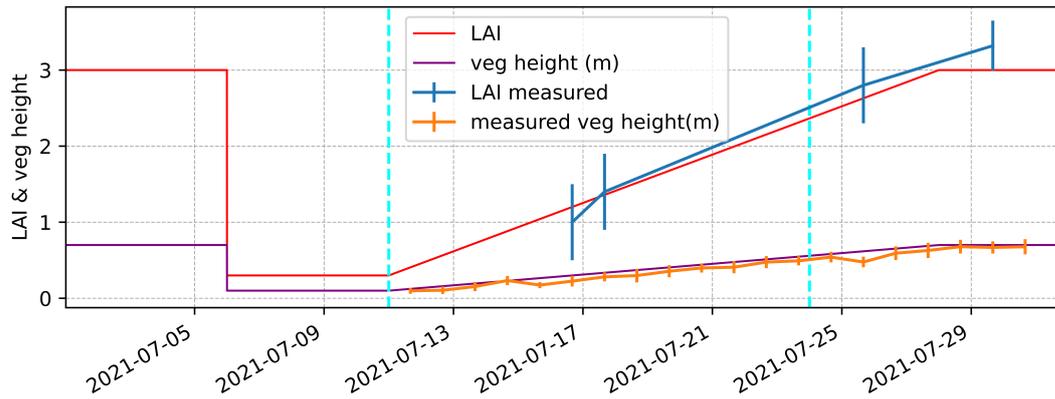
Figure 1. Cycle of cutting and growth of alfalfa at La Cendrosa site. Imposed Leaf Area Index (LAI) in red, measured LAI in blue, vegetation height in purple and measured vegetation height in orange.

4   Model configuration

4.1   Forcing data

The simulations of La Cendrosa and Els Plans are performed offline (i.e. driven by observations as input). They comprise the periods from 1 July at 00:00 UTC to 1 August at 00:00 UTC and from 17 June 10:00 UTC to 29 September at 09:00 UTC respectively. The associated atmospheric variables are the incident short and longwave radiation fluxes, wind speed, temperature, specific humidity, pressure, atmospheric CO_2 concentration, and rainfall rate at a 30 minute time step. All measurements were taken at 2 m except the wind which was measured at 10 m and precipitation that was measured at 1 m for both stations. The time evolving vegetation properties are usually imposed using a 10-day or monthly time step: for the current study, this temporal resolution is insufficient (more detail in Sect. 4.2.1). For Els Plans, several incidents in the availability of electric current after rain events resulted in gaps in the input variables. Short-wave radiation was gap-filled using a theoretical solar-zenith dependent method, and long-wave radiation gaps were filled using the correction proposed by Brutsaert (1975). The wind speed was filled with ~~the~~ an additional wind measurement at 3 m ~~data~~ at the same site, corrected by adjusting the wind speed to that which was already measured at 10 m above the surface assuming a logarithmic profile at neutral conditions. Pressure was gap-filled with a fixed average value during the same period. Since the albedo of the soil changes with the variation of the water content, values every 10 days are taken into account.

For La Cendrosa, irrigation was treated as ~~rain~~ rainfall by adding 30 mm of water ~~during two hours after~~ between 00:00 and 02:00 UTC. This approach introduces error for about four hours as it simulates an increase in evaporation of intercepted water over the leaves, the latent heat increases up to 130 W m^{-2} when vegetation is low and close to 70 W m^{-2} when it is high. The LAI and vegetation height cycle (shown in Fig. 1) cause the global albedo to change dynamically.
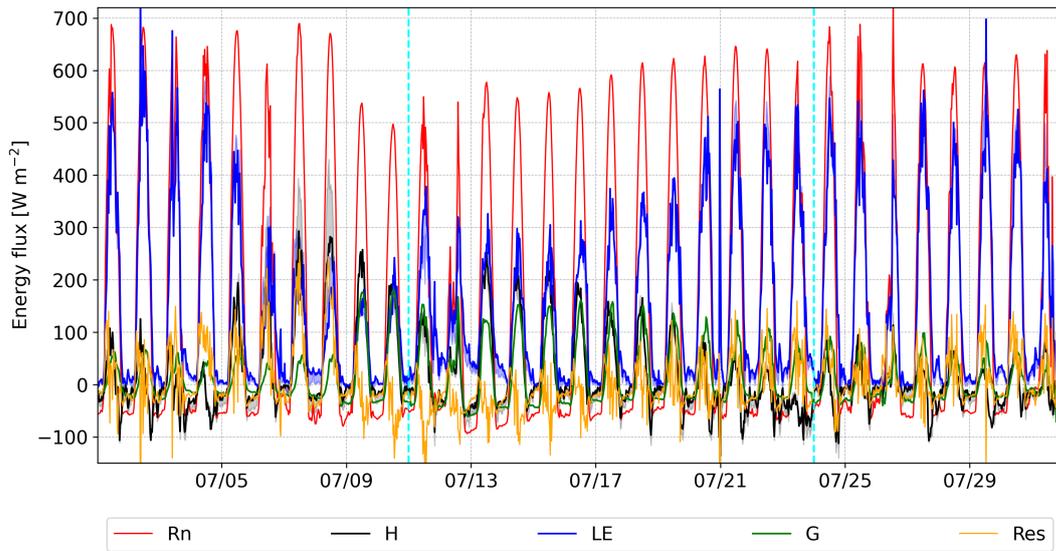
Figure 2. Observed terms of the Surface energy budget of La Cendrosa for the month of July 2021. In particular, Rn in red, H in black, LE in blue, G in green and the Res in orange. The gray and blue shading correspond to the error in the H and LE due to the Res, which is accounted for by the Bowen ratio. Cyan dashed lines indicate irrigation events and the gray line indicates the cutting of the alfalfa.
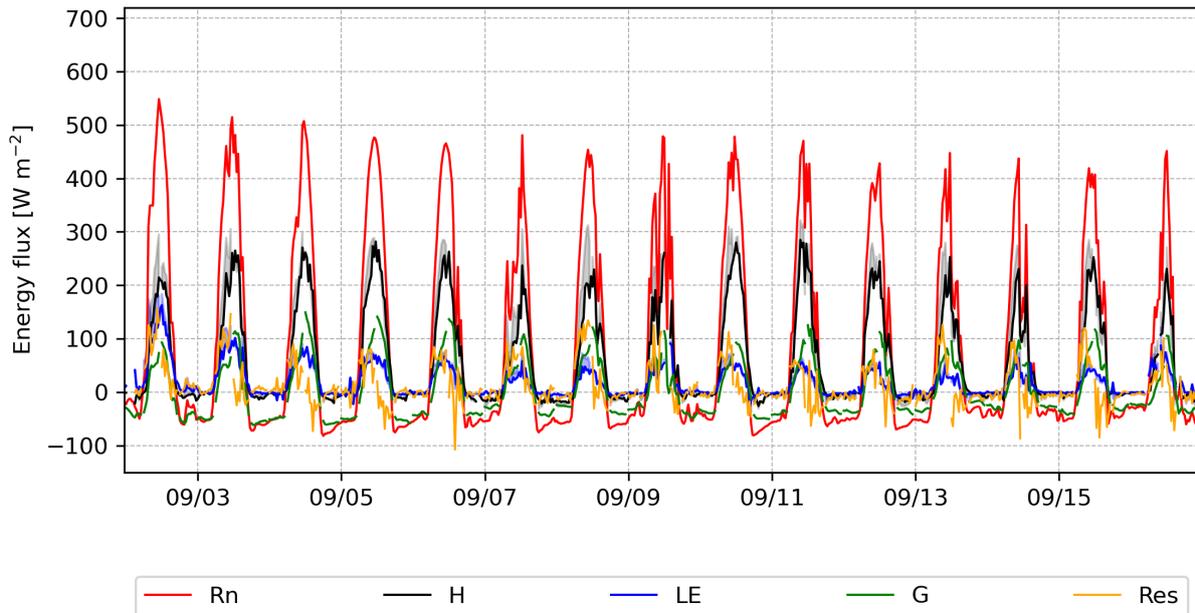

Figure 3. Observed terms of the Surface energy budget of Els Plans for a dry down period. In particular, Rn in red, H in black, LE in blue, G in green and the Res in orange. The gray and blue shading correspond to the error in the H and LE due to the Res, which is accounted for by the Bowen ratio.

4.2 Parameter selection

Table 1 shows the parameter values for the different model configurations. The prescribed dynamic roughness length (z_0) for both stations falls within the lower limits of the tabulated values in the literature (Oke 2002). For La Cendrosa, a single value is chosen as it gives reasonable estimates of the momentum for the whole period. The roughness length and the displacement height depend on the height of the vegetation but also on the density of the vegetation (Foken and Napo 2008), and the dependencies are still being parametrized (see the background in Jasinski et al. 2005) and are not currently modeled in ISBA, therefore a compensatory effect between the change on the two processes may be in play. For Els Plans, the roughness generating elements remain constant throughout the study period. The thermal roughness length (z_{0h}) is smaller at La Cendrosa, which shows less steep temperature profiles near the surface in the presence of dense vegetation. The emissivity values are within the error indicated by the tabulated values and have been left equal for both sites with a value of 0.97 (Snyder et al. 1998; Simó et al. 2019). However, it should be noted that the sensitivity to this parameter has been found to be low for this parameter for the ranges encountered at the two sites studied herein. For the type of vegetation of the alfalfa field, the C3 crop type is selected and C3 natural grass is used for Els Plans (Table 1).

4.2.1 Vegetation characterization of alfalfa

A realistic simulation of transpiration is the key to providing a good estimate of the LE, especially for the alfalfa. ~~It is dominated by several parameters that are best prescribed using observational data (if present).~~ The changes of LAI for La Cendrosa (Fig. 1) are imposed every time step compared to the original code since the alfalfa growth is relatively rapid (see Sect. 3.2). The height of the vegetation is modeled using a linear dependence on LAI based on the observations. Additionally, the AST option within SURFEX is used for both simulations. With this option, the A-gs scheme is used to model photosynthesis parameterizing its processes in contrast with other options that model transpiration directly without considering the biological processes. The vegetation can have either drought tolerant, Eq. (A9), or drought avoidant strategies, Eq. (A7), (Calvet et al. 2004). ~~The A-gs scheme is rarely compared with direct vegetation measurements (Van Diepen et al. 2022) because of the difficulty of finding a one-to-one equivalence for the parameters within the model.~~ Direct observations of stomatal conductance (g_s), CO_2 assimilation and photosynthetically active radiation (PAR) were made at la Cendrosa. ~~The mesophylic (g_m^*) and cuticular conductances (g_c), and the maximum assimilation (A_{max}) can be found from observations or via the maximum catalytic capacity of Rubisco (V_{cmax}), the enzyme that controls energy production. In contrast, quantum efficiency (ϵ_0) is usually a fitted parameter when the energy, assimilation and carbon curves are measured.~~ After testing multiple parameter configurations, it was found that increasing the quantum efficiency, ϵ_0, and the maximum assimilation (~~A_{max}~~ $A_{m,max}$(25)) gave results that reproduce results obtained with a higher cuticular conductance ~~. More energy than the default must be supplied to match the observed fluxes, regardless of whether it comes from the stomata or the cuticle. For this reason, the model adaptations are described below.~~ (see Appendix B1 for more details). The following changes to the vegetation parameters are imposed:

Table 1. SURFEX parameters characterizing the simulations of the Els Plans and La Cendrosa sites. In order, the dynamic roughness length (z_0), heat roughness length (z_{0h}), the number of soil layers, the SURFEX patch identifier (7 corresponds to C3 crops and 10 corresponds to natural grass), the range of leaf area index (LAI) and the height of the vegetation ($Hveg$) during the study period. *The strategy has been changed to drought-tolerant.

heightSite	z_0(m)	z_0/z_{0h}	soil albedo	veg albedo	soil layers	patch	LAI(m^2/m^2)	$Hveg$(m)
La Cendrosa	0.05	20	0.28	0.25	14	7*	0.3-3	0.1-0.7
Els Plans	0.01	1	0.19-0.25	0.25	25	10	0.1	0.2

Table 2. SURFEX parameters characterizing the soil properties of the Els Plans and La Cendrosa sites. The columns, in order, represent the depth (d), the sand and clay content, the water field capacity (w_{fc}), the wilting point (w_{wilt}) water content, the saturated water content ~~and soil porosity~~ (w_{sat}), the saturated hydraulic conductivity (K_{sat}), the b parameter of the CH78 pedotranfer function and the soil water potential at saturation, Ψ_{sat}.

Site	d (cm)	sand	clay	w_{fc}	w_{wilt}	w_{sat}	~~k_{sat}~~ K_{sat} (*10^{-5})	b	Ψ_{sat}
La Cendrosa	0-10	38.2/52.8	24.4/19.95	0.34	0.10	0.45	0.452	6.84	-0.33
La Cendrosa	10-30	56.0	15.5	0.28	0.10	0.43	1.488	5.62	-0.23
Els Plans	0-10	16.3	35.1	0.38	0.03	0.48	0.176/0.059	8.31/4.89	-0.51/-0.33
Els Plans	10-20	15.0	36.6	0.38	0.03	0.48	0.163/0.030	8.52/5.41	-0.52/-0.52
Els Plans	20-30	35.3	30.6	0.35	0.10	0.46	0.283/0.177	7.69/5.60	-0.35/-0.34
Els Plans	30-40	28.6	37.2	0.37	0.10	0.46	0.184/0.258	8.60/5.04	-0.40/-0.18

– Mesophyll conductance: ~~The PFT parametrization establishes the g_m^* through an associated curve that varies depending on whether the water use efficiency strategy under moderate stress is stress tolerant, Eq. (A9), or stress avoidant, Eq. (A7), and only one type is associated with each vegetation type (Calvet 2000).~~ Although alfalfa is a C3 crop, its drought strategy is tolerant as in C4 crops. Such plants species are known as C4-like species (Way et al. 2014). In consequence, the stress type has been changed to drought tolerant for the simulation. ~~For this site, the highest impact comes from the increase in absolute transpiration and not from the possible changes is stomata closure. With this strategy, parameters are set for generic species and must be modified to represent a particular species.~~ The g_m^* values have been changed to 0.005 $m\,s^{-1}$ (see Table B1). ~~These values are within the observed values of the control (Aranjuelo et al. 2013) and lower values would correspond to stressed alfalfa. Lower values of 0.00197 $m\,s^{-1}$ were also observed with unstressed alfalfa (Malik et al. 2018). For the CLASS model (De Arellano et al. 2015), González-Armas et al. (2023) used a g_m^* value of 0.01 $m\,s^{-1}$ which was found for the same site. After setting the other parameters, the differences in mean error and root~~

mean square error modifying the g_m^* value from 0.005 to 0.1 m s^{-1} in SURFEX are below one W m^{-2} for all fluxes. Differences arise on the days on which stomatal closure is simulated and depend on what degree the closure is effective. It should be noted that alfalfa is bred for the development of drought/salinity tolerant varieties that are thus optimized for cultivation in arid and semi-arid regions of the Mediterranean area (Mouradi et al. 2022). However, the modification of this parameter is necessary, but there are still errors in the estimation of ET so additional parameters are explored.

– Cuticular conductance: As a first approximation, increasing the cuticular conductance to 0.0006 m s^{-1} provided good estimates of ET. Measurements of cuticular conductance can follow several strategies and give different values for the same species (Kerstiens 1996). Simplification to a minimum value of conductance ($gmin$) and other similar values such as nocturnal conductance or detached leaf conductance are more commonly measured (Duursma et al. 2019), $gmin$ values are more similar to values of g_c which serve as a default in numerical simulations and are used as a proxy. For alfalfa, the value was set to $0.00007 m s^{-1}$ according to Kerstiens (1996). When used, it provided simulations with a profound dip in evaporation in the central part of the day, resulting in unrealistic results compared to observations. No further values of g_c for alfalfa were found in the literature, which could probably indicate the difficulty of measuring this parameter. The Kerstiens (1996) value is one order of magnitude below the tested value of $0.0006 m s^{-1}$ and three times less than the default value in SURFEX of $0.00025 m s^{-1}$. The default value has been used as it is closer to the literature value without being outside the typical observed values of this parameter for other vegetation. Values up to at least $0.006 m s^{-1}$ can still provide reasonable estimations of ET but are outside the reported values and they ar non-physical. This behavior is given by the relationships from equations (A16) and (A5), which holds the sum of g_c and g_m^* in the denominator and can compensate the effects from one another. Together with Eq. (A10), an increase of g_c produces a similar effect to increasing g_m^*.

– Quantum efficiency: The ϵ_0 can be directly related to the increase in transpiration, an increase of ϵ_0 in Eq. (A20) induce an increase in carbon assimilation in Eq. (A19) and of the stomatal conductance, Eq. (A10). This parameter is based on the theoretical quantum requirement of photons needed to assimilate one molecule of CO_2 (Von Caemmerer and Farquhar 1981) , and it limits the assimilation rate (see review in Van Diepen et al. (2022)). Goudriaan et al. (1985) presents a revised value of 0.017 mg CO_2 J^{-1} and suggests that selective breeding of the plant species could lead to an increase in this value in new varieties. Its value has not evolved in the SURFEX configuration over the years. There is some evidence that this value is variable; Collatz et al. (1992) showed a small temperature dependence and Cai and Dang (2002) identified a variability of this parameter within tree species, but the exploration of this parameter in measurements has seemingly not progressed in recent years for meteorological applications. Mouradi et al. (2022) and Jiang et al. (2009) show that depending on the alfalfa variety, the electron transport rate and the PAR conversion efficiency (biological measurements used by their community) can be increased, apparently exploiting an increase in electron efficiency, although no direct conversion to these parameters has been found. This efficiency will decrease during drought events (Zhang et al. 2019; Mouradi et al. . Thus, the ϵ_0 value used may be more variable than reported and may have been compensated by an increase in other

parameters such as cuticular conductance. The ~~ϵ_0 value of~~ value of $0.0265\,\mathrm{mg}\,CO_2\,\mathrm{J}^{-1}$ found by González-Armas et al. (2023) increases the LE to values closer to the observed values and is therefore used in this study.

- – Maximum assimilation: ~~The A_{max} sensitivity is most relevant for low LAI values, as marginal increases of this value will be weighted more heavily to increase transpiration than for other parameters. The relationship of $A_{m,max}$ in Eq. A14 has a nonlinear response for g_s. The increase of $A_{m,max}(25)$ in Eq. (A18) increases A_n in Eq. (A19) and on to the stomatal conductance, Eq. (A10), but $A_{m,max}$ can also be found in the denominator.~~

  ~~The default value of $A_{m,max}(25)$ is 2.2 mg. For alfalfa, both higher values (Bunce 2018) with 2.64 mg, which were transformed from V_{cmax} as in Collatz et al. (1991), and lower values (Malik et al. 2018) of 1.4 mg have been reported in the literature.~~ González-Armas et al. (2023) found values (3.02 mg) at La Cendrosa that were considerably higher than those given in the literature and the standard value in SURFEX. Increasing this value in this simulation improves the transpiration estimates for days that show a dip in ~~ET~~ LE during the day reducing its intensity, therefore the value in González-Armas et al. (2023) is kept, but the default values are adequate for most of the simulated days.

An extended version of this section is in Appendix B1 with detailed justification over the parameter changes and its bibliographical context.

4.2.2 Vegetation characterization of drying grass

For Els Plans, the choice of LAI is complex. Measurements of LAI at the site have a median value of $0.34\,\mathrm{m}^2/\mathrm{m}^2$ and a minimum value of 0.12 ~~$\mathrm{m}^2/\mathrm{m}^2$~~ m^{-2} (Brooke 2023). However, these measurements take into account the shaded area and do not necessarily represent active vegetation. In contrast, in ISBA LAI is taken as green LAI and therefore represents fully active vegetation (Brut et al. 2009). This does not correspond well with the measurements in Els Plans, where the vegetation is dying but still provides shade and intercepts moisture. Furthermore, this shade comes from the blades of the natural grass rather than the leaves. The value of ~~$LAI{=}0.1$~~ $LAI = 0.1$ ~~$\mathrm{m}^2/\mathrm{m}^2$~~ m^{-2} is used as a compromise to take into account the shaded ground and part of the dry vegetation that does not contribute to evaporation, thus limiting transpiration.

A complementary parameter necessary to characterize the vegetation is vegetation height ($Hveg$), which tests show is not a highly sensitive parameter for either site and is set to $0.2\,\mathrm{m}$ by rounding the observed value of $0.16\,\mathrm{m}$ for Els Plans. In healthy active low vegetation such as crops, LAI may not be directly related to its height or it may depend on the crop so they are set independently (Yuan et al. 2013).

4.2.3 Soil characterization

Table 2 lists the measured sand and clay content values together with the soil hydraulic parameters obtained from the soil texture data and the pedotransfer function from Clapp and Hornberger (1978), referred to herein as CH78. For la Cendrosa, two surface measurements of the soil characteristics were carried out by different teams. The first was near the position of the SEB station with two levels, the second was about $20\,\mathrm{m}$ away within the same field. It was observed that the second measurement had proportions of sand and clay close to those at a depth of 10-30 cm of the first measurement. Since the field is

irrigated by flooding, some washing of the soil can take place, which can be the source of these near-surface discrepancies in texture between the samples of the different teams. The two-level measurements are used for La Cendrosa for all parameters except wilting point of the model, which is reduced to include the minimum water content within the root zone which is seen in the observations. At the Els Plans site, a more extensive sampling of the soil was performed and incorporated, so that the matric potential at saturation Ψ_{sat}, the slope of the retention curve b and the saturated hydraulic conductivity K_{sat} values were fitted from soil core samples using the HYPROP method (Shokrana and Ghane 2020) and $Ksat$ values were measured in the laboratory. The Ψ_{sat} value differed from that given by CH78 at the surface and bottom of the soil profile and the b parameter is at the lower end of its range. Using these vertically-varying observed values reduced the overall error of the simulation compared to using a constant values for the vertical profile of the soil and compared to the default values taken from the global database. This matches the results of Sobaga et al. (2023) who identified that the default b parameter produced a lack of drainage in SURFEX V8.1. K_{sat} is taken as the observed value instead of the fitted one, as it also leads to an improvement in the LE and H estimation. We note that it differs by an order of magnitude at the surface. Soil layers deeper than those observed were assumed to have the same soil properties as that in the lowest observed layer. The discretization of the soil layers has been chosen to match the layers to the depth of the observations, while maintaining the highest vertical resolution near the surface of the soil column.

4.2.4 DSL parameters

The DSL configuration for the main comparison is the one of Swenson and Lawrence (2014) but its parameters may not be the most suitable for ISBA. A sensitivity analysis, consisting in the variation of two parameters for the DSL resistance is later presented. This kind of analysis is necessary to characterize the changes of output variables and diagnose them. The response to the change can be identified, whether it is linear, nonlinear or negligible. As the number of parameters increases, the behaviours of outputs become intertwined and cannot be necessarily easily predicted. The sensitivity analysis identifies whether a parameter is relevant for a certain variable. We generate multiple simulations with two varying parameters and use the root mean square error (RMSE) of the simulations to suggest the more appropriate values for the estimation of the turbulent fluxes with ISBA for the DSL option.

5 Results/Discussion

This section presents an analysis of the simulations carried out for La Cendrosa and Els Plans using the default and new soil resistance parametrizations. The different simulations are identified by the names NON, S92 and DSL to indicate no soil resistance, the use of Sellers 92 resistance and a DSL resistance, respectively.

According to Foken and Napo (2008), a bulk indication of instrumental errors indicates that Rn can have errors of around 10 %, errors in H and LE can reach 20 %, together with a 50 % error for the G, not accounting for the energy storage error. Note that budget closure is not necessarily a measure of the quality of the fluxes (Aubinet et al. 2000). The lack of closure in observations is expressed as residual energy. It includes part of the instrumental error, but also owing to horizontal advection

due to heterogeneity (not modeled), heat storage due to vegetation and its exchanges (modeled in ISBA-MEB but considered small compared to soil storage under normal circumstances), and unmeasured phase water changes in the soil (not modeled) (Cuxart et al. 2015).

As mentioned in Sect 3.3, the local sea breeze reduces the residue, so some advection contribution to the residue is expected. Consequently, the main analysis concentrates on the comparison of fluxes with the simulation without imposing closure on the observed fluxes but the statistical comparison is also shown with the closure imposed by the Bowen ratio method (Barr et al. 1994).

5.1 The simulated energy budget

Table 3 shows the statistical comparison of the energy budget for La Cendrosa, divided into three time periods; daily, daytime and night. The distinction between daytime and night is made from 8 a.m. to 8 p.m., leaving out the more complex changes of the transitions in the night period since the main changes caused by the use of a resistance occur during the day. The following analysis focuses on the daytime, so that behaviors resulting from certain periods, such as low and high vegetation or flooding events, can be identified. A comparison of the simulated and observed Rn is shown in Fig. 4 a and e. Despite the mean error (ME) indicating a bias close to zero, the NON simulation is positively biased overall, and this behavior is improved through the use of the DSL scheme. In particular, two days show a different trend that modifies the statistics (Table 3). This behavior corresponds to the period between the cutting and the removal of the alfalfa, which took place a few days later. The effect that the resistances have on the Rn is mainly due to the difference in the longwave energy budget and surface temperature, since less heat is emitted in the NON simulation by the soil, and the albedo input does not change between simulations. The LE flux shown in Fig.s 4 b and f is centered on the one-to-one line, with a subset that is deviating from the one-to-one line corresponding to the period of low vegetation with relatively low LAI after the irrigation period. The improvement in LE is shown by a reduction in ME, ~~root mean square error (RMSE)~~ RMSE and an increase in correlation (see Table 3). For the H, the larger errors are corrected with the use of a resistance to compensate for the change in LE. The improvement of the statistics is also present for H ~~and the underestimation is reduced~~, with the underestimation being reduced, and the RMSE reducing to $37\,W\,m^{-2}$ for La Cendrosa and $45\,W\,m^{-2}$ for Els Plans. These values are within the values of the standard deviation observed for the residue for La Cendrosa ($56\,W\,m^{-2}$) and Els Plans ($50\,W\,m^{-2}$). On the other hand, the simulated soil stores more energy and releases it faster than observed, with a daily cycle characterized by a hysteresis effect that overestimates during the day and underestimates at night thus worsening the results for G. The resistance also impacts the nighttime statistics with a reduction of the Rn that results in a lower available energy at night, and an small increase of ME and RMSE for LE and H of the order of $1\,W\,m^{2}$.

At the Els Plans site, the Rn is well represented by the imposed albedo (Fig. 5). The error of Rn (Table 4) remains well below the $10\,\%$ error of the measurement. The use of a DSL resistance increases the RMSE and ME up to $2\,W\,m^{-2}$. For the LE, the scatter is large in all three simulations compared to its absolute value, with a delay in the start of evaporation and an underestimation with absolute errors close to 50%. The RMSE of LE is reduced during the daytime from 29 W m^{-2} to 19 W m^{-2} using the DSL approach. The correlation is best for the S92, followed by the NON simulation, and closely by the

DSL simulation as in this case the LE is too damped. The sensitivity to the parameters used is discussed in Sect. 5.4. For the H there is a small reduction in the RMSE but an increase in the ME, so the overall performance remains the same except for an improvement from ~~0.81 to 0.88~~ 0.87 to 0.89 in the overall correlation. For the G performance, the intense heating of the soil is again simulated with hysteresis, with the transfer of energy being quicker in the model than that observed (Fig. 5d and h), which corresponds to a daily RMSE of ~~57~~70 W m^{-2} (Table 4). No measurements of the thermal properties of the soil have been made, and so the default properties assigned to the observed soil texture have been taken. A sensitivity test indicated that reducing the thermal conductivity of solids in the soil by 25~~%, value within the range of different soil types reviewed from observations by Zhang and Wang (2017), %~~% could reduce this error by reducing the G flux up to 20 W m^{-2}, while increasing the error in the H proportionally. This value is within the range of different soil types reviewed from observations by Zhang and Wang (2017). Overall, due to the higher error in the measurements of G, estimated at 50%, this bias in the simulation is considered tolerable. The change of Rn and H at night due to the resistances is the same as for La Cendrosa, but in this case, LE has an small improvement of the correlation of approximately ~~0.08~~0.02, with a nearly negligible change in the overall average LE value.

5.2 The latent heat flux

The observed LE is shown for the aforementioned simulations in Fig. 6a together with a top to bottom barplot with rain and irrigation. The largest change between simulations is after the first irrigation event [July 11]. The increase of observed LE is overestimated with the NON option, mainly due to the large contribution from soil evaporation, as in ~~(Lohou et al. 2014)~~ Lohou et al. (2014), whereas the LE in the DSL simulation is reduced more rapidly, which matches more accurately the observations in this period. The ~~other irrigation event~~ second irrigation event [July 24] and small rain events result in small increases in LE that decreases during the hours after as the soil is still near saturation and have little impact on the available water. The difference in the maximum LE between irrigation events is due to the change in transpiration. The first event presents very low vegetation whereas the second is fully grown alfalfa.

Estimates during periods of high LE are well captured by all three simulations, and it is slightly better for the NON simulation, than for the S92 and DSL simulations since the reduction of soil evaporation is not compensated by increased transpiration. The differences range from 5 to 10% as the soil dries. LE is also well represented for the low vegetation period for the three simulation types. The soil resistance reduces the contribution of soil evaporation to LE resulting in an improvement in the RMSE of LE (daily) of 16 W m^{-2} for the S92 simulation and 20 W m^{-2} for the DSL simulation (see Table 3).

The nocturnal LE values show good agreement with the observations, except for nights with a higher flux, in which the simulations underestimate the value (e.g. ~~July 8th~~8 July). The simulations respond well to small rain events such as the night of the 21st but with a more moderate increase. Such an increase occurs artificially in the simulation for the first irrigation event reaching 130 W m^2, as irrigation was imposed as rain, but returns to the observed values after five hours.

For Els Plans, the interruption of the measurements after rain events mentioned in Sect. 4.1 affected the number of dry-down periods that were well captured, limiting the analysis of such events. Such a period is shown where the maximum LE is better captured by S92 in Fig. 6 b compared to the NON or DSL. Although this is after a rain event, the H is dominant and the

Table 3. Mean Error (ME) and Root Mean Square Error (RMSE) in W m^{-2} for the net radiation (Rn), the sensible heat flux (H), the latent heat flux (LE), and the ground heat flux (G) for La Cendrosa site. In brackets is the modified value. The correlation (Corr) between simulation and observation has been included for H and LE. The values taking into account the residual using the Bowen ratio method are indicated in brackets.

daily	ME Rn	RMSE Rn	ME H	RMSE H	Corr H	ME LE	RMSE LE	Corr LE	ME G	RMSE G
NON	0.67	31.65	-4.44 (-18.06)	45.90 (55.19)	0.81 (0.84)	16.51 (-10.43)	65.85 (70.70)	0.93 (0.92)	-10.80	56.68
S92	-2.46	29.21	-0.49 (-14.11)	39.09 (47.70)	0.88 (0.91)	8.25 (-18.68)	50.03 (62.58)	0.95 (0.94)	-9.62	60.99
DSL	-5.49	28.00	4.52 (-9.10)	37.11 (43.86)	0.88 (0.90)	-0.68 (-27.61)	46.70 (65.04)	0.95 (0.94)	-8.73	64.90
daytime	ME Rn	RMSE Rn	ME H	RMSE H	Corr H	ME LE	RMSE LE	Corr LE	ME G	RMSE G
NON	7.35	41.09	-18.85 (-33.83)	59.75 (73.76)	0.80 (0.83)	35.49 (-1.84)	87.22 (86.64)	0.87 (0.86)	-1.69	64.88
S92	3.01	37.32	-12.03 (-27.01)	49.55 (63.01)	0.88 (0.90)	19.10 (-18.23)	64.28 (73.96)	0.92 (0.90)	3.55	70.28
DSL	-0.76	35.02	-4.47 (-19.45)	45.70 (57.20)	0.87 (0.89)	3.04 (-34.29)	58.64 (77.27)	0.92 (0.91)	8.28	75.02
night	ME Rn	RMSE Rn	ME H	RMSE H	Corr H	ME LE	RMSE LE	Corr LE	ME G	RMSE G
NON	-6.68	17.25	10.18 (-2.17)	24.65 (23.81)	0.83 (0.86)	-4.35 (-21.04)	28.93 (49.20)	0.89 (0.84)	-18.49	48.60
S92	-8.55	17.52	11.08 (-1.27)	24.47 (23.25)	0.85 (0.87)	-4.12 (-20.80)	27.55 (48.54)	0.90 (0.85)	-21.49	51.75
DSL	-10.78	18.53	13.39 (1.04)	26.15 (23.74)	0.82 (0.84)	-5.56 (-22.25)	29.10 (49.87)	0.89 (0.84)	-24.59	54.43

Table 4. Mean Error (ME) and Root Mean Square Error (RMSE) in W m^{-2} for the net radiation (Rn), the sensible heat flux (H), the latent heat flux (LE), and the ground heat flux (G) for Els Plans site. In brackets is the modified value. The correlation (Corr) between simulation and observation has been included for H and LE. The values taking into account the residual using the Bowen ratio method are indicated in brackets.

| daily	ME Rn	RMSE Rn	ME H	RMSE H	Corr H	ME LE	RMSE LE	Corr LE	ME G	RMSE G
NON	-4.33	11.39	12.06 (-15.54)	45.37 (62.00)	0.92 (0.89)	2.80 (-5.04)	22.13 (23.92)	0.77 (0.75)	-7.35	70.05
S92	-4.75	11.79	12.69 (-14.91)	44.00 (60.66)	0.92 (0.90)	1.83 (-6.00)	15.71 (21.41)	0.81 (0.75)	-7.32	73.39
DSL	-5.17	12.23	13.72 (-13.88)	44.50 (60.88)	0.92 (0.90)	0.34 (-7.50)	15.37 (22.75)	0.78 (0.72)	-7.36	76.28
daytime	ME Rn	RMSE Rn	ME H	RMSE H	Corr H	ME LE	RMSE LE	Corr LE	ME G	RMSE G
NON	-2.76	14.04	16.12 (-22.08)	57.91 (76.81)	0.87 (0.84)	5.88 (-3.73)	28.54 (28.80)	0.74 (0.73)	-7.48	81.61
S92	-3.02	14.43	16.52 (-21.68)	55.66 (74.71)	0.89 (0.86)	4.35 (-5.26)	19.58 (24.96)	0.77 (0.71)	-6.53	85.97
DSL	-3.29	14.83	17.53 (-20.67)	55.98 (74.79)	0.89 (0.86)	1.64 (-7.97)	19.02 (26.94)	0.72 (0.65)	-5.31	89.71
night	ME Rn	RMSE Rn	ME H	RMSE H	Corr H	ME LE	RMSE LE	Corr LE	ME G	RMSE G
NON	-6.18	7.75	6.49 (-10.79)	26.99 (44.09)	0.89 (0.88)	-0.71 (-6.83)	12.75 (17.98)	0.61 (0.58)	-4.03	58.71
S92	-6.77	8.24	7.41 (-9.88)	27.39 (44.07)	0.89 (0.88)	-1.35 (-7.46)	10.40 (17.58)	0.69 (0.66)	-4.73	60.92
DSL	-7.32	8.76	8.42 (-8.87)	28.47 (44.65)	0.88 (0.88)	-1.58 (-7.70)	10.64 (18.14)	0.72 (0.68)	-6.01	62.83
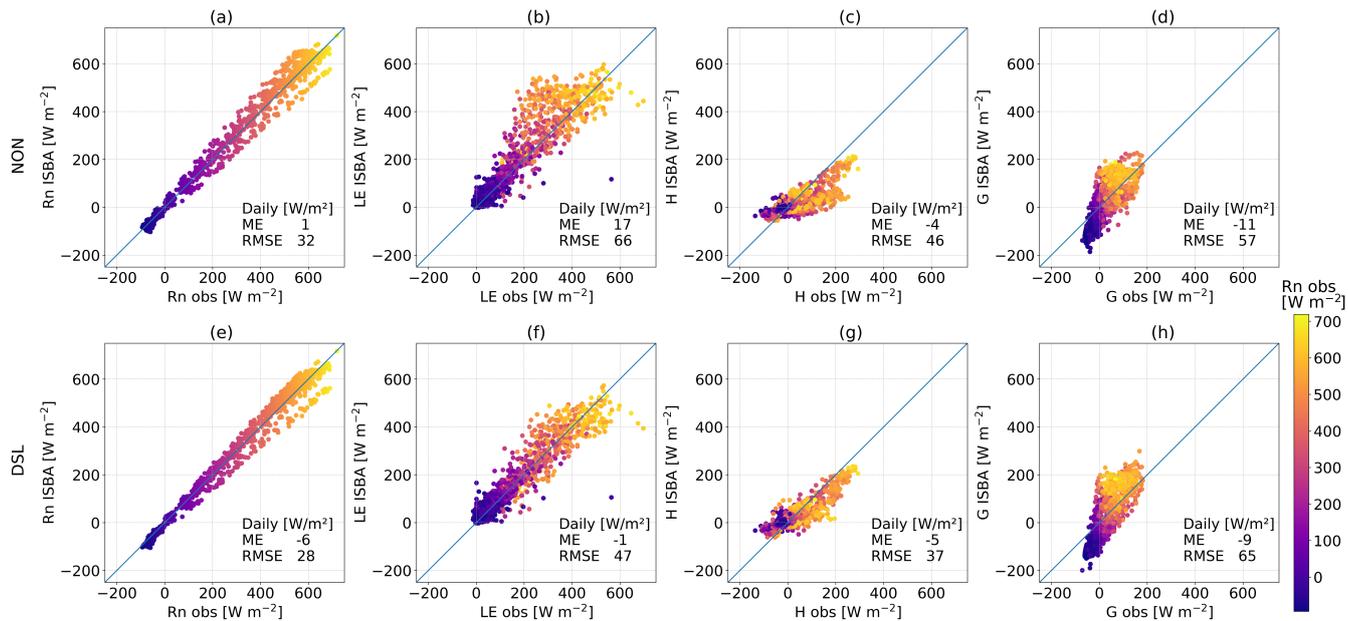
Figure 4. Scatterplots of the simulated terms of the energy budget against the observation for La Cendrosa site for the NON simulation (NON, a-d) and the DSL simulation (DSL,e-h). From left to right, Rn (a,e), H (b,f), LE (c,g), and G (d,h). The simulation period is from July 1 at 00 UTC to August 1 at 00 UTC. Daily mean error and root mean square error are included in the figure frame.
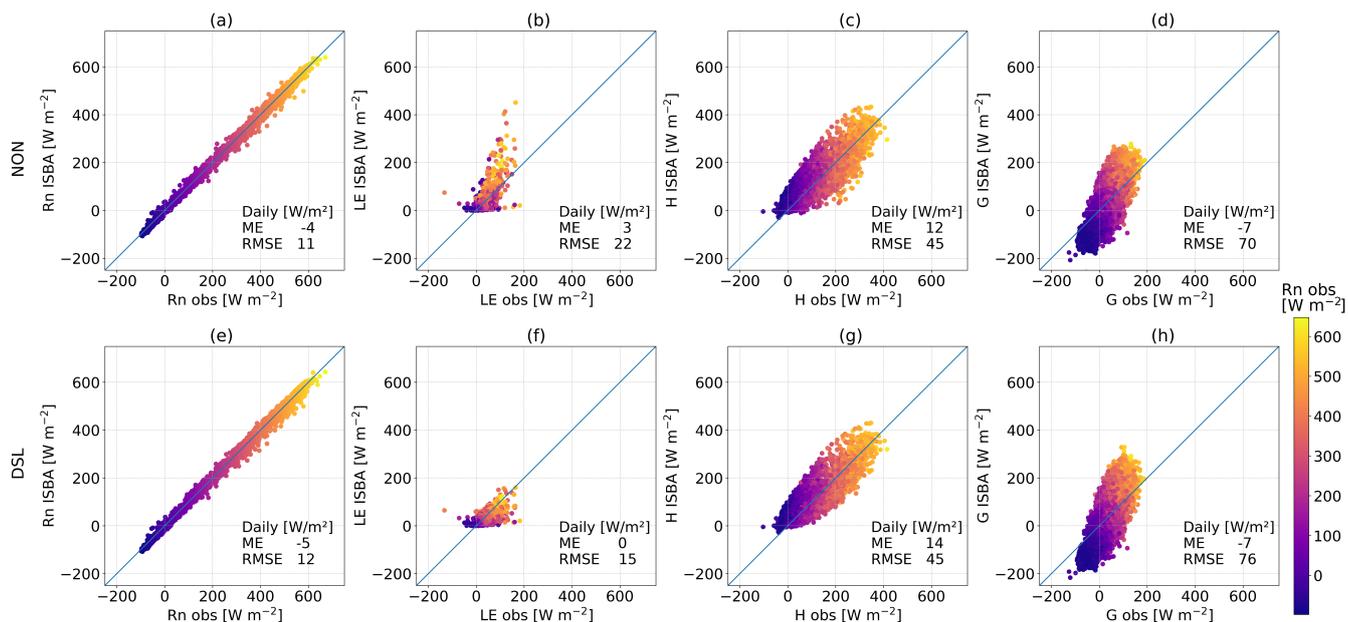

Figure 5. Scatterplots of the simulated terms of the energy budget against the observation for Els Plans site for the simulation with no resistance (NON, a-d) and simulation with the DSL approach (DSL,e-h). From left to right, Rn (a,e), H (b,f), LE (c,g), and G (d,h). The simulation period is from June 17 10 UTC to September 29 at 9 UTC. Daily mean error and root mean square error are included in the figure frame.

magnitude of LE is small. The vegetation at this site is mostly senescent, and the water content of the first soil layers is very low. Following a rain event, soil evaporation increases and contributes significantly to ET throughout the day. Evaporation from the interception is also present in the model for about six hours and increases up to $10\,\mathrm{W\,m^{-2}}$. However, as the soil dries, bare soil evaporation contribution is present only in the middle hours of the day. Instead, the main contribution is attributed to the dying vegetation and shows a slower daily cycle with a slower progression in the increase in ET. The modeled transpiration values are on the order of $30\,\mathrm{W\,m^{-2}}$ compared to the daily maximum of LE of $50\,\mathrm{W\,m^{-2}}$. Nonetheless, they represent only a relatively small part of the energy budget and are of the order of the residue. For Els Plans the nocturnal observations show that negative LE values are common at night, indicating dew formation or soil water vapor adsorption, which is typical not only under such dry conditions (Paulus et al. 2024; Kohfahl et al. 2021), but also under more humid soil conditions (Groh et al. 2018a). The presented simulations have struggled to reproduce these negative values, because the soil temperatures are high and the transition to a stable regime is rare.

5.2.1 Soil resistances

Modeled soil resistances are at their minimum values after rain or irrigation events and increase with time as the soil dries. For La Cendrosa site (Fig. 7a), the soil resistance value increases using the DSL approach and resistance values can reach up to four times that of S92. Note that the DSL resistance does not start acting until the VWC has fallen below saturation to the w_{dsl0} threshold, unlike the S92, which always presents some resistance.

In the case of Els Plans, the resistance values of the DSL simulation remained continuously above the value of S92, and increased by a factor of almost 2 (Fig. 7b). Generally, rainfall events were not abundant enough during the summer season with high evaporative demand to reduce the resistances to zero at this site. Although they were significantly reduced at times, the arid conditions were persistent throughout the summer months.

The resistance values estimated for Els Plans are similar to those found in Swenson and Lawrence (2014), while those of La Cendrosa are higher, due to the difference in soil properties. The increase in resistance starts earlier than observed in laboratory studies (Zhang et al. 2015). Their values were closer to the S92 simulation, but slightly higher and remained lower than those shown for the DSL simulation. These differences result in limited change in LE as there's little water available in the soil, since the VWC is much lower than the field capacity. In addition, Balugani et al. (2023) found that a DSL observed under natural conditions can be larger than that measured in a lysimeter, whether in laboratory or field conditions. The higher values for resistance compared to the ones by Zhang et al. (2015) may be explained by the exposition to the atmospheric conditions which will affect ET, soil moisture and soil temperature profile (Balugani et al. 2023). To explore this further, a sensitivity analysis is carried out in the following section to test the optimal parameter configuration.

5.2.2 Water Storage

To study the longer term effects of using a soil resistance, Fig. 8a shows the cumulative water loss and its decomposition into transpiration and soil evaporation at La Cendrosa. The differences in cummulative ~~LE~~ E loss between the various simulations are small before the vegetation is cut, up to 3 mm (2%). The LE is underestimated in all three simulations and the simulated
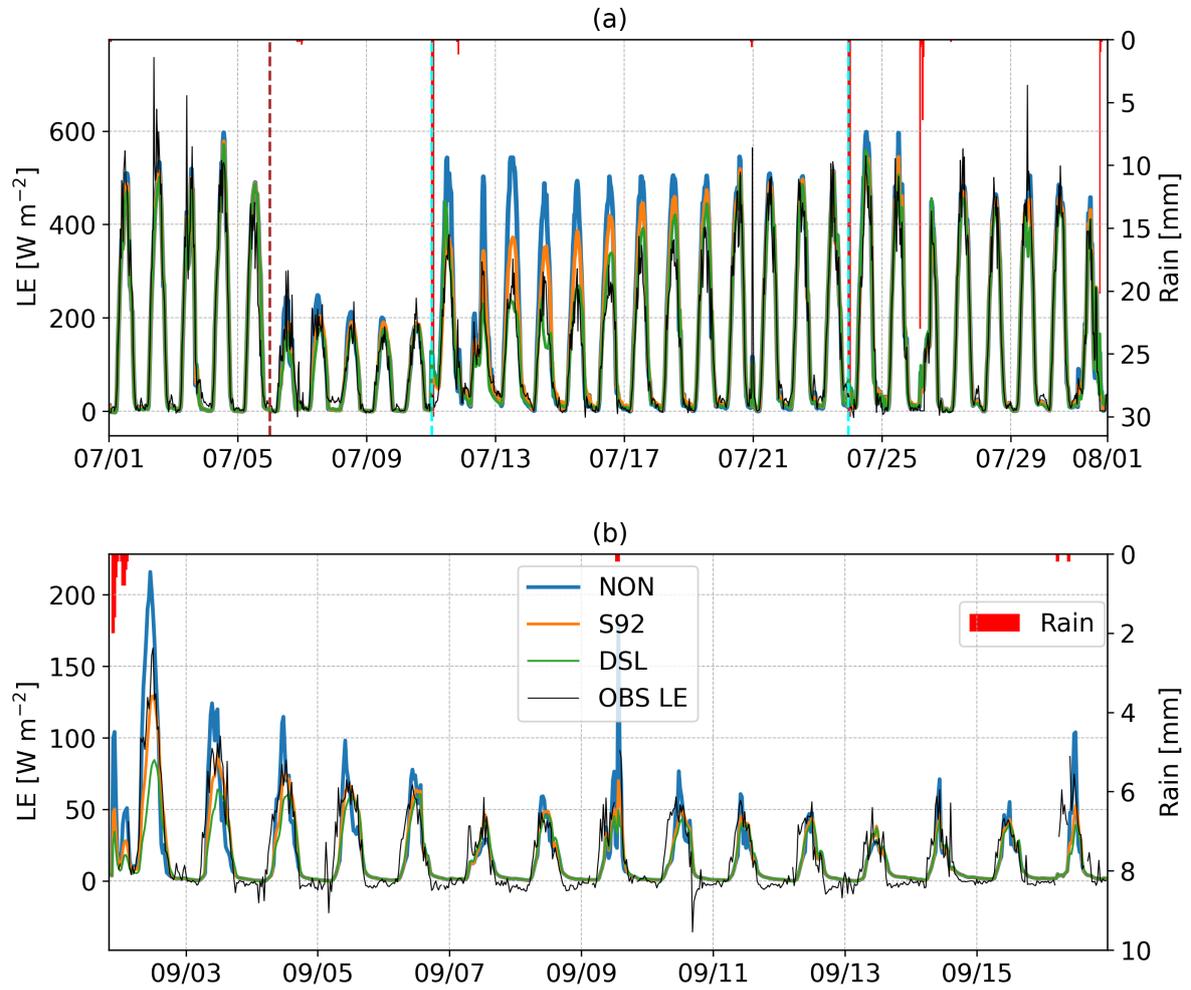
23

Figure 6. Observed (black) and simulated latent heat flux (LE) timeseries of La Cendrosa (a) and for Els Plans sites (b) for the simulations with no resistance (NON, blue), with a Sellers 92 resistance (S92, orange) and a DSL resistance (DSL, green). Bar lines represent the rain. Vertical lines represent the vegetation cut (brown) and irrigation (cyan).
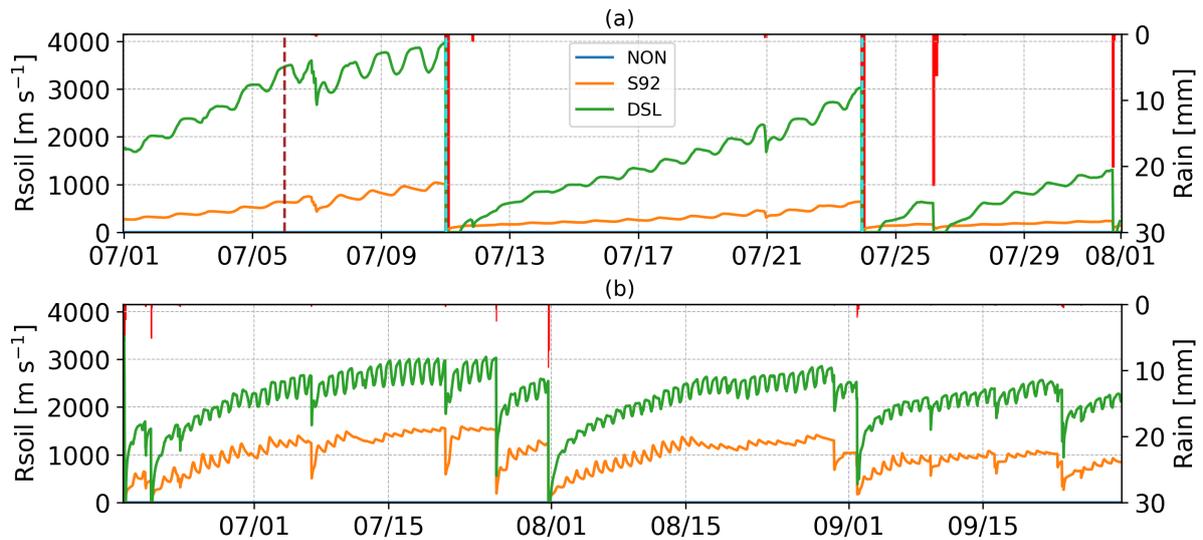
Figure 7. Simulated soil resistance timeseries of La Cendrosa (a) and for Els Plans sites (b) for the simulations with no resistance (NON, blue), with a Sellers 92 resistance (S92, orange) and with a DSL resistance (DSL, green). Bar lines represent the rain. Vertical lines represent the vegetation cut (brown) and irrigation (cyan).

transpiration dominates until the alfalfa harvest on July 6. Thereafter, a first trend change is observed, which is reproduced by all three simulations. After the irrigation event of the 11th of July, a second change in tendency occurs for which transpiration increases slightly, but soil evaporation increases significantly the following days, the strength of which is determined by the resistance applied to the simulation (Fig. 7). The LE in the DSL simulation initially underestimates ~~ET~~ E slightly, but recovers

590   during the growth period and matches the ~~LE~~ E trend at the end of the period, falling within 1 mm difference with respect to observations. The other two simulations accumulate an excess water loss of 9 mm for S92 and 19 mm for NON due to the overestimation of bare soil evaporation. Estimation of the partitioning can be made for ~~July 29th~~ 29 July at this site as an estimate of the ratio between transpiration and ET for daytime was made on ~~July 29th~~ 29 July using microlysimeter and EC measurements. The observation gives a ratio of 0.87 for this day. The simulations for DSL gave ratios closest to the

595   observations with a ratio of 0.88. The NON simulations resulted in a much lower ratio (0.66), showing that the contribution of soil evaporation to total ET is significantly overestimated without DSL. However, it should be noted that the NON simulations can reach values up to 0.85 for other days.

   For the four months analyzed at Els Plans, the minimum ~~ET~~ cumulative change was determined to be in July. After a significant rain event in early August, the ~~ET~~ E rate increased as more water was available. Fig. 8b shows the ~~cumulative ET~~ E

600   and the partitioning of the model. It is important to note that we are at the limits of the model for representing ~~ET~~ LE with the current LAI formulation of SURFEX. LAI is used to represent the density of photosynthetically active vegetation. For this site, there was a shading effect and the thermal inertia due to the vegetation mass was high, but a very limited transpiration.

These effects are not well taken into account due to their dependence on LAI and its low value to represent the small part of active vegetation, and thus the soil flux is also accentuated for this site by the model.

In spite of these difficulties, the simulation with a DSL manages to reproduce the ~~ET~~ cumulative evaporated water at the beginning of the period and mostly matches the tendency during the summer months. The split between transpiration and bare soil evaporation may be biased towards more transpiration than occurred in reality as estimations of ~~ET~~ LE in similar conditions can be of only 10% (Ma et al. 2020), but they are within the realm of possibility as senescent leaves have been reported to be limited to transpiration of 0.1 mm h^{-1} (Pérez-Anta et al. 2024). The presence of gaps in the measurements of ~~ET~~ LE within the rainy period did not allow the observation of the increase of the cumulative evaporated water during periods with infiltration. The cumulative water during the driest period near the 15th of July was underestimated by 4 mm and by 10 mm for the DSL and NON simulations, respectively, during the SOP. At the end of September, the cumulative ~~ET~~ evaporated water overestimation is slightly reduced to 1 mm and 9 mm for the DSL and NON simulations, respectively. A small amount of resilient vegetation was observed to germinate at the end of August, which may explain the additional LE and reduction of the model bias. The ~~ET~~ LE values for this period are low enough that the observational uncertainty of ~~ET~~ LE can explain a large part of these differences. Nevertheless, it is noteworthy that the change in the trend of evaporation in August in the observations corresponds to the beginning of the period of germination of sporadic natural grasses at the Els Plans site.

When comparing the sites, the difference in the amount of water evaporated between the two sites is remarkable. In one month at La Cendrosa, the amount of water evaporated is three times greater than that accumulated in more than three months at Els Plans: irrigation significantly alters the water balance of the area.

5.3 Other relevant variables

5.3.1 Albedo

The observed daily variability of albedo and its model counterpart are shown for La Cendrosa in Fig. 9a. The standard deviation shown is from the 30 minute time series of the observations and the simulation. The observed albedo values varied by more than 0.1 during the month of July. The alfalfa albedo variability has been reported to be up to 0.2, depending on the solar angle (Al-Yemeni and Grace 1995). The change is linked to alfalfa leaves which track the solar angle: they cup and reduce the albedo (Travis and Reed 1983). This process occurs in conjunction with a midday decrease in leaf water potential (Bell et al. 2007).

Model albedo is obtained through a constant imposed value for both surface albedo and vegetation albedo. It was chosen to provide a more accurate R_n so that the available energy of the model remained accurate for the other fluxes. ISBA-MEB modifies this initial value taking into account LAI and solar zenith angle. The model reproduced then part of the cycle, but its amplitude was weaker than the measured one, changing by at most 0.03. Observations show that alfalfa has albedo values close to 0.16 when fully grown, while after cutting the surface albedo increases to values close to 0.22, varying with vegetation growth and VWC. As albedo was forced with daily varying values in the current study, modelling the absorption in MEB through the canopy captures some of the changes due to growth from the 9th to the second irrigation period, the 24th. In Fig. 9b, the albedo of Els Plans is influenced by the dryness of the soil, varying with the formation of the DSL and the
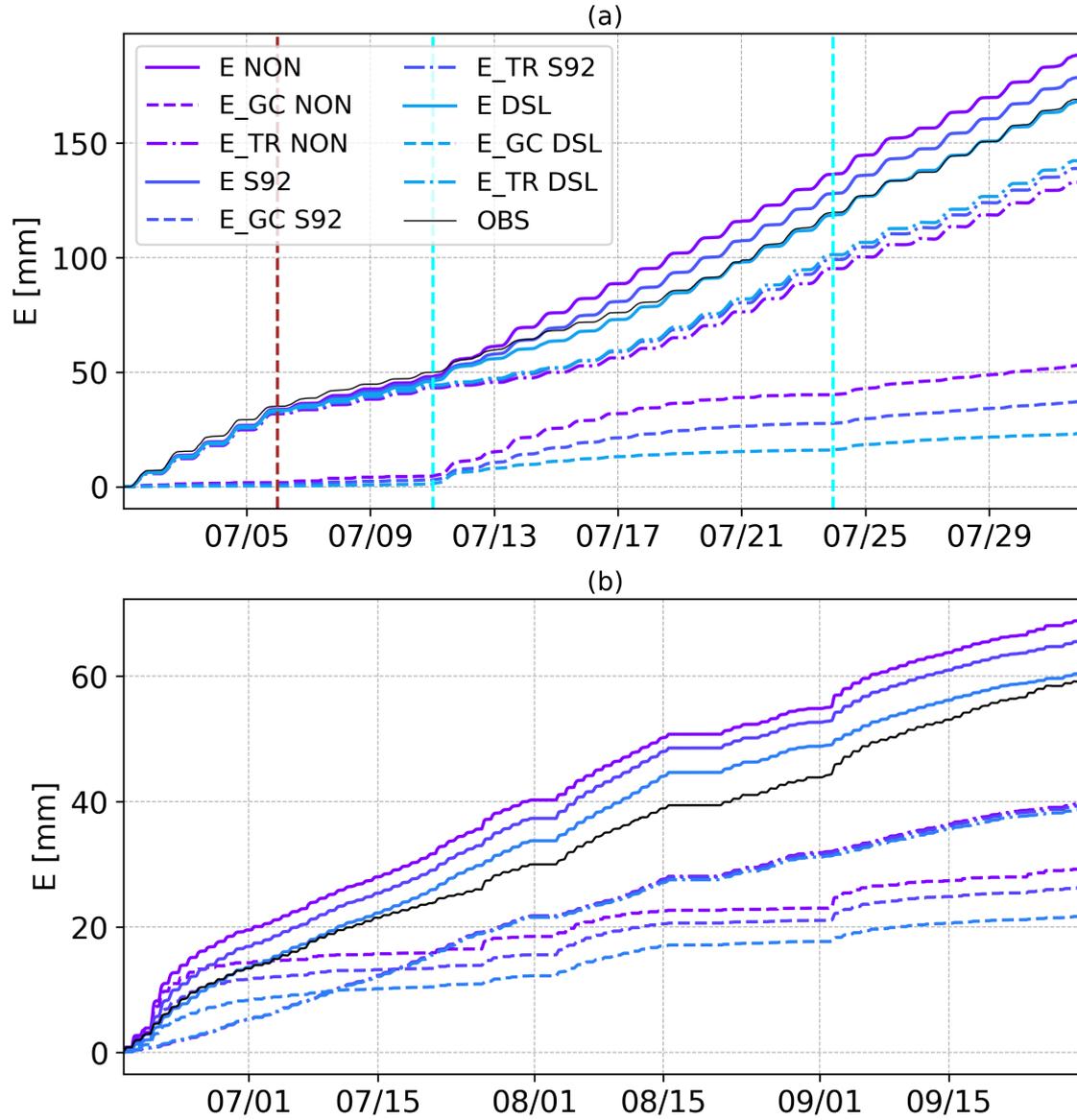
Figure 8. Accumulated latent heat flux ($\underset{\sim}{LE}E$) for La Cendrosa (a) and Els Plans sites (b). Observations are in black, simulations with no resistance are in purple, with Sellers 92 in deep blue and a DSL resistance in cyan. Solid lines correspond to the $\underset{\sim}{LE}E$, dashed lines correspond to the ground evaporation and dashed and dotted lines correspond to the transpiration contribution. The vertical brown line corresponds to the harvest, and cyan lines correspond to irrigation events.
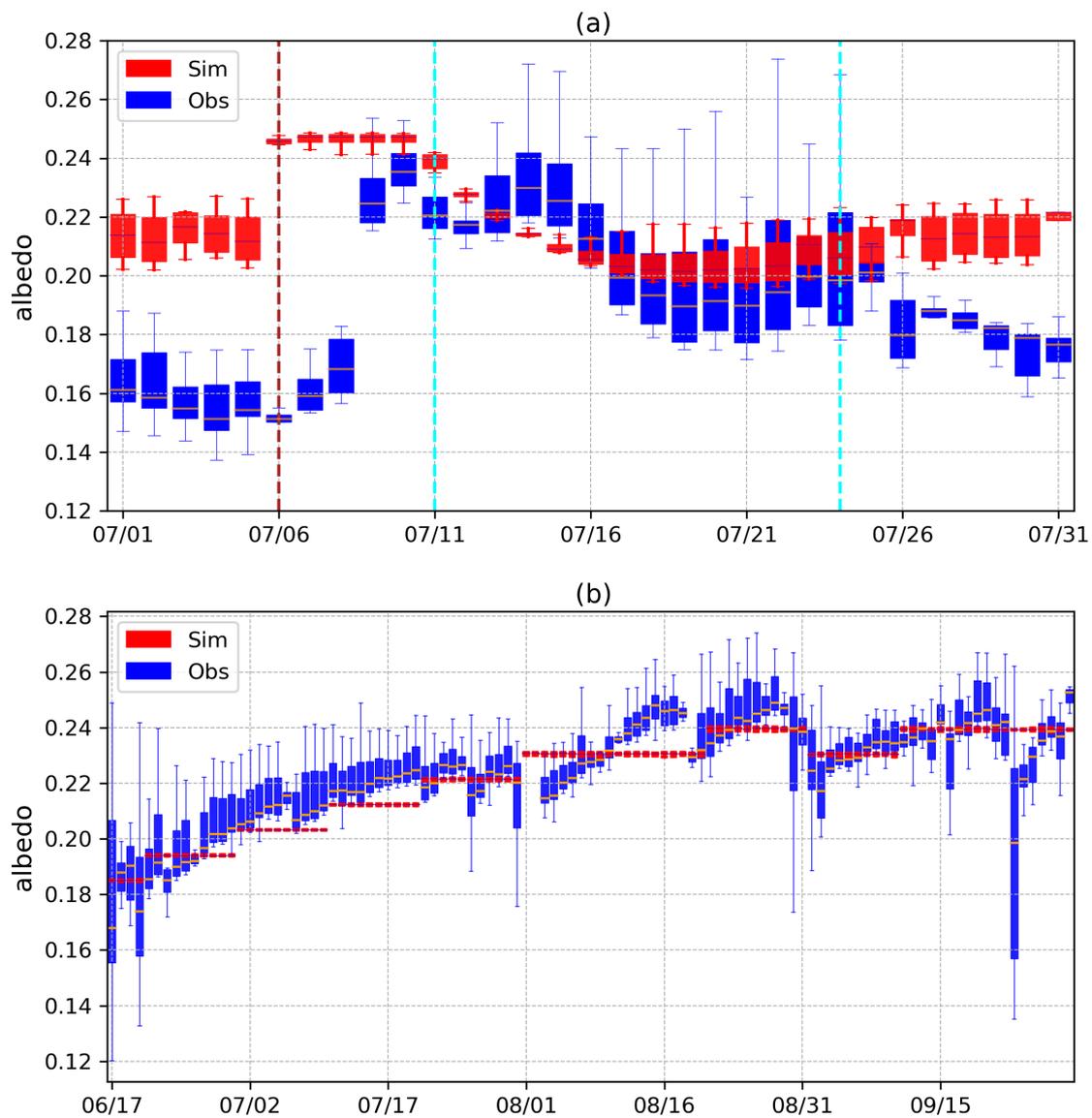
Figure 9. Observed (blue) and simulated (red) albedo for the NON simulation for La Cendrosa (a) and Els Plans sites (b). Each boxplot measurement shows a central line with the median value. The size of the boxes correspond to the quartiles of albedo observations within the day and the error bars to the variability of the albedo within the day.

reduction in VWC in accordance to what De Silans et al. (1989) and Van de Griend and Owe (1994) have observed under bare soil semiarid conditions. The change in albedo over the LOP ranged from 0.18 to 0.25, which is consistent with the findings of Béziat et al. (2013), who found an albedo of 0.25 for senescent crops which are expected to be close to senescent natural grass. The observed rain events reduced soil albedo by up to 0.03, between before and after the events. The decadal prescription of the albedo is not enough to capture this variation. Due to the low LAI, no daily cycle is included in the simulation of Els Plans although a sub-daily variability of albedo is observed. These differences do not generate a large discrepancy in the Rn.

5.3.2 Volumetric water content

The VWC dynamics are highly tied to LE, and ISBA attempts to represent this linkage through several mechanisms. The amount of transpiration is limited by D_{max}, Eq. (A6), through the water stress factor f_2 in Eq.(A8), and bare soil evaporation by VWC, Eq. (3). The addition of a soil resistance, such as the DSL resistance, adds an additional dependence of LE on the VWC, that limits further ET when the VWC is scarce.

Reproduction of VWC dynamics is highly dependent on soil hydraulic properties obtained for the site La Cendrosa from soil texture data and a pedotransfer function. The observations of VWC at La Cendrosa (Fig. 10a) present a soil moisture profile that does not decrease with depth, but rather has a layer at 10 cm that reacts very quickly to precipitation or irrigation events. This shows that drainage after precipitation or irrigation is significantly faster than for observations at 5 cm or 30 cm. This layer has a much higher sand content which, combined with a lower field capacity and a higher $Ksat$, results in faster infiltration of water into deeper soil layers. This layer seems to coincide with the point at which the number of roots begins to decrease, as seen when the sensors were installed. This could mean that in drier conditions in the topsoil (-5 cm), root water uptake can decrease rapidly. Soil samples were taken at depths of 0 to 10 cm and 10 to 30 cm and the analysis data (Table 1) show that there is a strong change in sand content and $Ksat$ at 10 cm depth. The large difference in the observed VWC and drainage dynamics after the events suggests that the probe represents the depth between 10 and 30 cm. The fast response of the VWC during rainfall and irrigation events might indicate that water was transferred along spatially distinct pathways (preferential flow) in the soil subsurface (Guo and Lin 2018).

The VWC in ISBA is simulated using the mixed-form of the Richardson equation, and thus it can model heterogeneous vertical texture or soil property profiles. In the current study, it was found that changing the soil hydraulic parameters representing the uppermost five layers (0-13.5 cm) to have a higher sand content at the first two layers and lower for the other three significantly impacts the soil properties, and the observed profile with a more humid 10 cm level can be better reproduced (not shown). Current soil world databases predict the superficial layer up to 5 cm to a resolution of 250 m (Hengl et al. 2017) and are used by multiple global models (Vereecken et al. 2019). But as seen by the difference in sand content of the two surface soil surface layer measurements from Table 2, the spatial variability of the soil is high at this site. Measurements within the field close to the EC-tower showed for the top layer (0-10 cm) a much higher sand content (56%) compared to the observations at another location in the same field (38%) from Table 2. In consequence, the parameters have been left as those indicated in Table 2. The simulation has a positive bias of 5% during irrigation flood events caused by a lack of drainage, but the model is able to capture the tendency of the VWC for the DSL simulation. Note that for the NON simulation, this tendency is

670 underestimated. Although the absolute value is closer to observation for the period before July 24, the rate of loss of water has to be correct for proper LE estimation, and it is thus prioritized over absolute value, which is driven by the field capacity value and which has been calculated with soil samples with CH78 pedotransfer functions. Furthermore, the values of VWC probes can be subject to biases due to the type of probe and manufacturing (Jackisch et al. 2020). The rapid response of the water content at all three observation depths following the flood irrigation event probably indicates that some of the water is

675 being transferred to deeper soil levels via preferential flow pathways in macropores (Nimmo et al. 2025). Implementing a dual permeability approach, as described by (Gerke and Van Genuchten 1993), could improve the simulation of water flow using the Richards equation in fractures (macropores) and the matrix (micropores) in the future but such changes still face challenges for the implementation at larger scales. After the 24th of July, when the vegetation is almost fully developed, the differences between these simulations remain small, but the differences against observation remain large.

680 For Els Plans (Fig. 10b), the same bias is observed in terms of the trend. The absolute value of the NON simulation being closer to observation for 5 and 10 cm, but deviates significantly from the observation for 30 cm. Here, the DSL appears to capture the redistribution of water following a rainfall event more accurately than the NON, as too much water is used in this approach for soil evaporation. The tendency is larger for the NON simulation than for the observation. For the DSL the tendency is too strong on the wetting events, following what was observed for LE, and giving further necessity for a sensitivity test of

685 the resistance. The difference between the simulations becomes increasingly larger for ~~the~~ each soil water content level, which are reduced after rain events. The re-wetting of the deeper layer (i.e., 30 cm) only occurs for the largest rainfall event on the 31st of July as a delayed response, since the top soil layer was very dry and water was mainly used to refill the soil water storage and thus could not infiltrate deeper than 10 cm for the other events. The simulations showed a delayed response compared to observation when water infiltrated to the 30 cm layer. Despite the more extensive measurements of soil hydraulic parameters,

690 some potentially important processes, such as flows through cracks or macropores (preferential flow paths) are currently not included in the model structure. In general, the use of pedotransfer functions or laboratory measurements may not be suitable for determining soil hydraulic properties for a specific site. Weihermüller et al. (2021) showed that the choice of pedotransfer function can have a large impact on soil water dynamics, so using an ensemble mean instead of a specific pedotransfer function can be a good solution to reduce this uncertainty (e.g. Krevh et al. 2023). A better method is the inverse estimation of soil

695 hydraulic parameters based on observations of soil water dynamics for the different layers, which significantly reduces this parameter uncertainty. However, this requires sufficient in situ observations of VWC and matric potential (Groh et al. 2018b; Schübl et al. 2023), which determine the field water retention characteristic, as well as sufficiently long time series that include drying and re-wetting phases. A study of this kind was carried out with SURFEX v8.1 by Sobaga et al. (2023), in which drainage was assessed and improved. Its functions are still being migrated to V9, so the observational derived parameters were

700 given priority in this study.

5.3.3 Soil temperature

The diurnal cycle of soil temperature measured at 5 cm in La Cendrosa (Fig. 11a) has an amplitude of about 5°C on most days. Before irrigation, when the vegetation is very low, it reaches a maximum of about 10°C. In contrast, the simulations
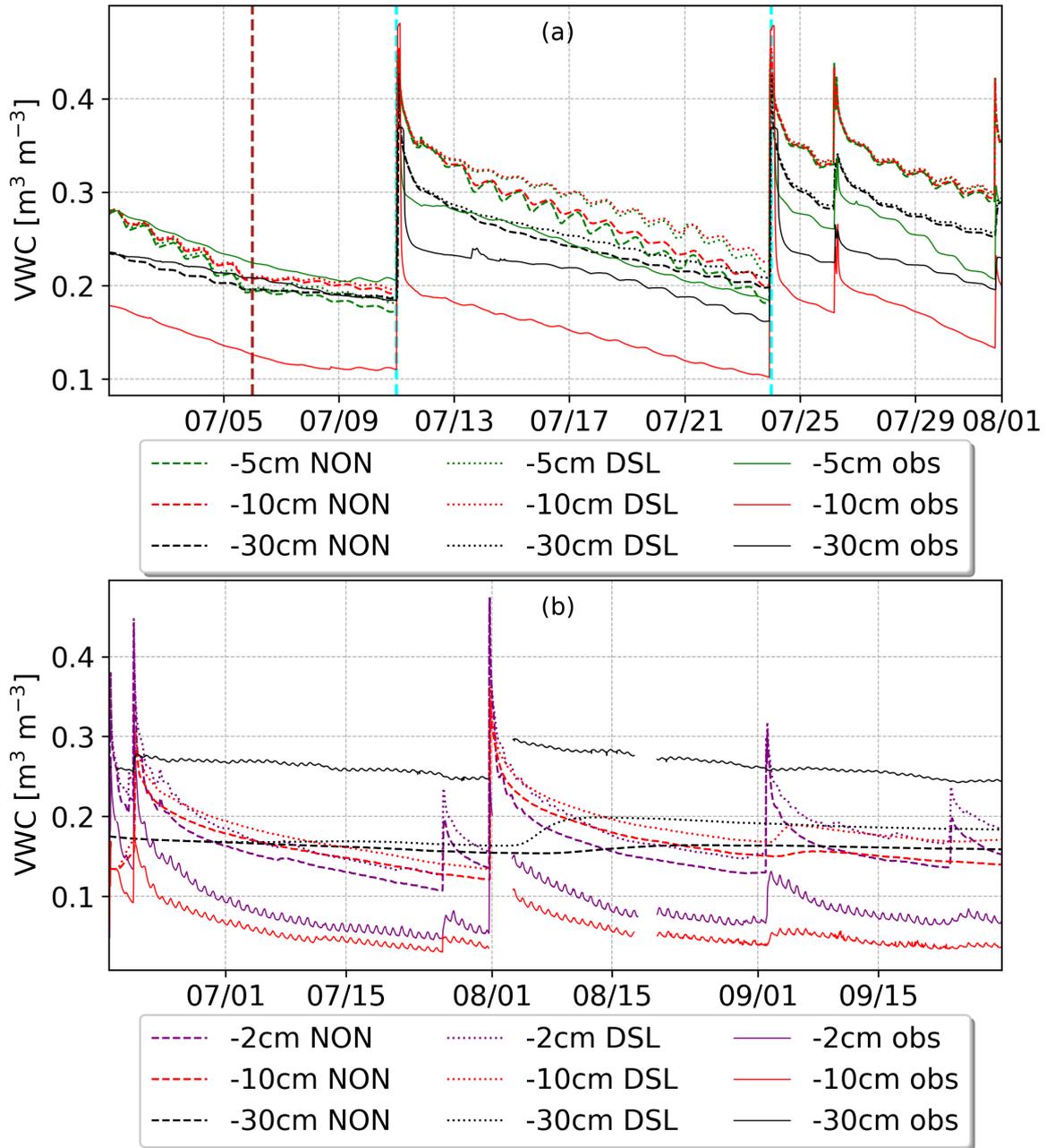
Figure 10. Volumetric water content (VWC) of the soil at La Cendrosa site (a) and Els Plans (b) sites at different depths. Levels comprise 2, 5, 10 and 30 cm depending on the availability for the site. Observed VWC is shown in solid lines, the NON simulation in dashed lines and the DSL simulation in dotted lines.
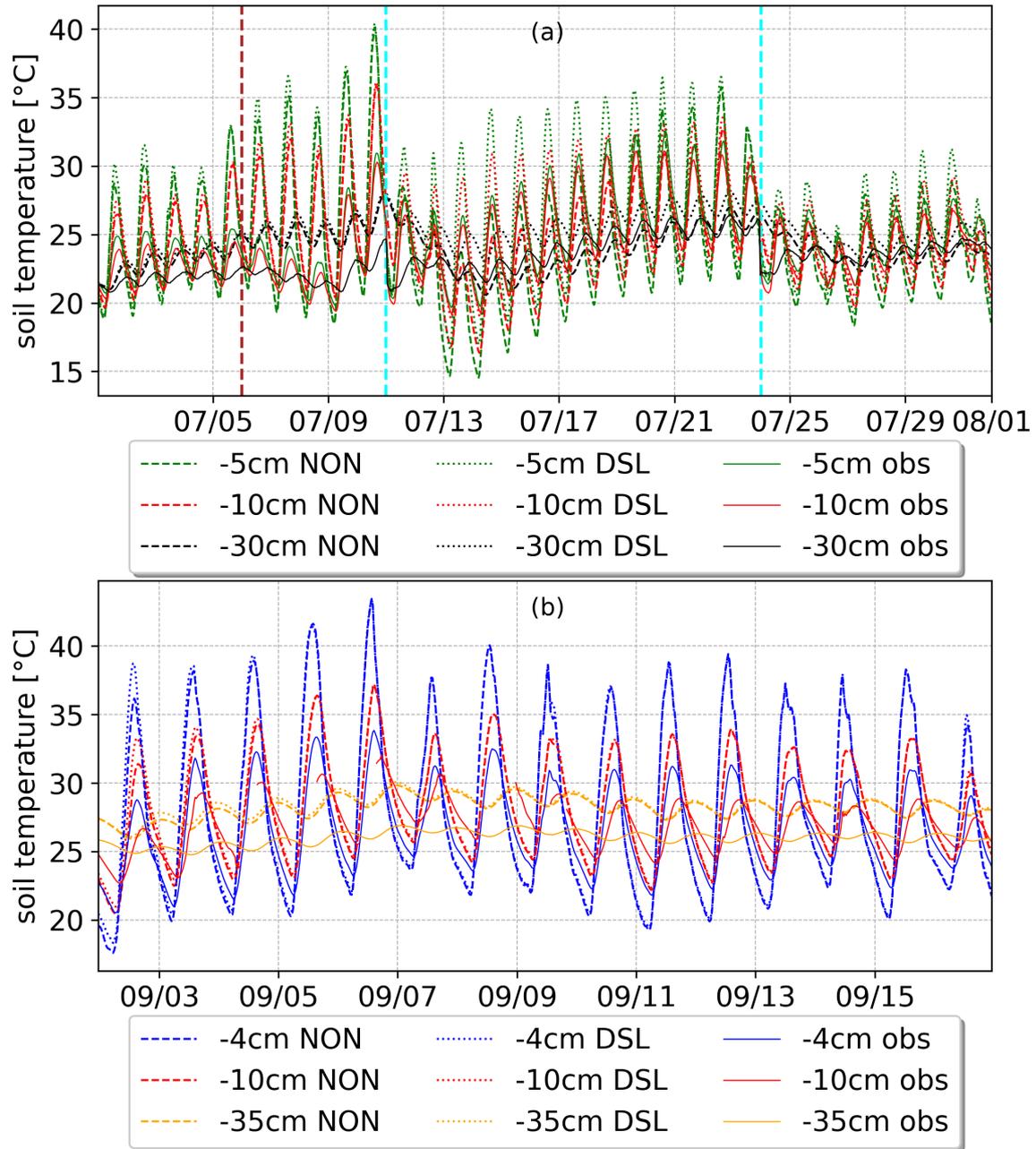
Figure 11. Soil temperature at La Cendrosa site (a) and Els Plans (b). Levels comprise at 4, 5, 10, 30 and 35 cm depending on the availability for the site. Observed temperature is shown in solid lines, the NON simulation in dashed lines and the DSL simulation in dotted lines.

have a larger amplitude at the beginning. After irrigation, the NON simulation better reproduces the soil temperature diurnal pattern, the DSL simulation increases the temperature at 5 cm up to 5°C in response to the increase in G due to the decrease in LE. Interaction between the atmosphere and the ground is insufficient and heat is stored instead of being transformed into sensible heat. While the roughness length could be increased to reduce this effect, the characterization of LE would be impacted negatively. For Els Plans, Fig. 11b), shows a period of drying. At the beginning, when water is more available, the differences between the NON and the DSL simulations was up to 2°C, leveling off when soil moisture at the surface layer reduces over time. The layers below 5 cm show the greatest differences, while the temperature at 10 cm maintains a maximum difference of 5°C throughout the period. These differences indicate that the thermal conductivity is too high. Attempts to reduce the amplitude of soil temperature, such as the inclusion of the impact of soil organic matter on the soil thermal properties, reduce the bias but do not completely correct it and do not correspond to a realistic characterization of the soil at the site. In order to remain as close as possible to the real behavior of the global application of the model, no change has been made to the thermal conductivity. Strategies such as a variable thermal conductivity of the first layer dependent on its thickness such as for the CLM model (Swenson and Lawrence 2014) could be adopted if a pattern is identified for larger domains.

5.4 Parameter sensitivity analysis

The parametrization of a DSL resistance depends on parameters that have uncertain values, as the formation of a DSL depends on the type of soil, but also on other soil properties that are often unknown. The parameters K_{dsl} and z_{dsl} are assumed to be the most important since small variations can change the global ET (Swenson and Lawrence 2014) by over 10% as they modulate the onset of a DSL and the rate of its growth, respectively. Therefore, a sensitivity analysis of K_{dsl} and z_{dsl} was performed for both sites during the daytime since this is when the ground resistance should have the largest impact on ET. The RMSE of the estimated fluxes for La Cendrosa (a,c,e,g) and Els Plans (b,d,f,h) for a range of values of z_{dsl} and K_{dsl} during the daytime is shown in Fig. 12 for the approach with an DSL. Changes in z_{dsl} produce a linear effect as the resistance changes in magnitude, whereas the effect produced by changes in K_{dsl} is non-linear and it is proportional to the saturation value of the soil.

For Rn, the optimal values of RMSE for La Cendrosa and Els Plans in Fig. 12 a and b are in the opposite extremes of the tested sensitivity values, but the RMSE change . The RMSE value which compares the default DSL simulation shown in the previous section to the optimal value is very low, between 4 W m^2 for La Cendrosa and 2 W m^2 for Els Plans.

For La Cendrosa, the improvement with higher resistance comes from the days after the irrigation period, where the Rn is overestimated and the decrease in LE is compensated by a rise in H and G together with a reduction of the longwave emission that reduces the positive bias. For Els Plans, for days when the soil remains dry, the simulation with a larger DSL resistance value shows a greater Rn compared to simulations with a lower resistance value, whereas under humid conditions, the opposite is true. The increase in error in Rn with an increasing resistance value depends on several factors and not on a specific period.

For the LE and H fluxes, it can be observed that values of K_{dsl} below 0.6 degrade the simulations compared to the proposed DSL values of Swenson and Lawrence (2014) (daytime in Tables 3 and 4). In Sect. 5.1, it was observed that although the DSL simulation produced better results than the simulation without a resistance (NON), the damping of evaporation was greater than optimal for both sites. This is consistent with the sensitivity tests where values of LE with a width resistance of $z_{dsl} = 0.01$ m
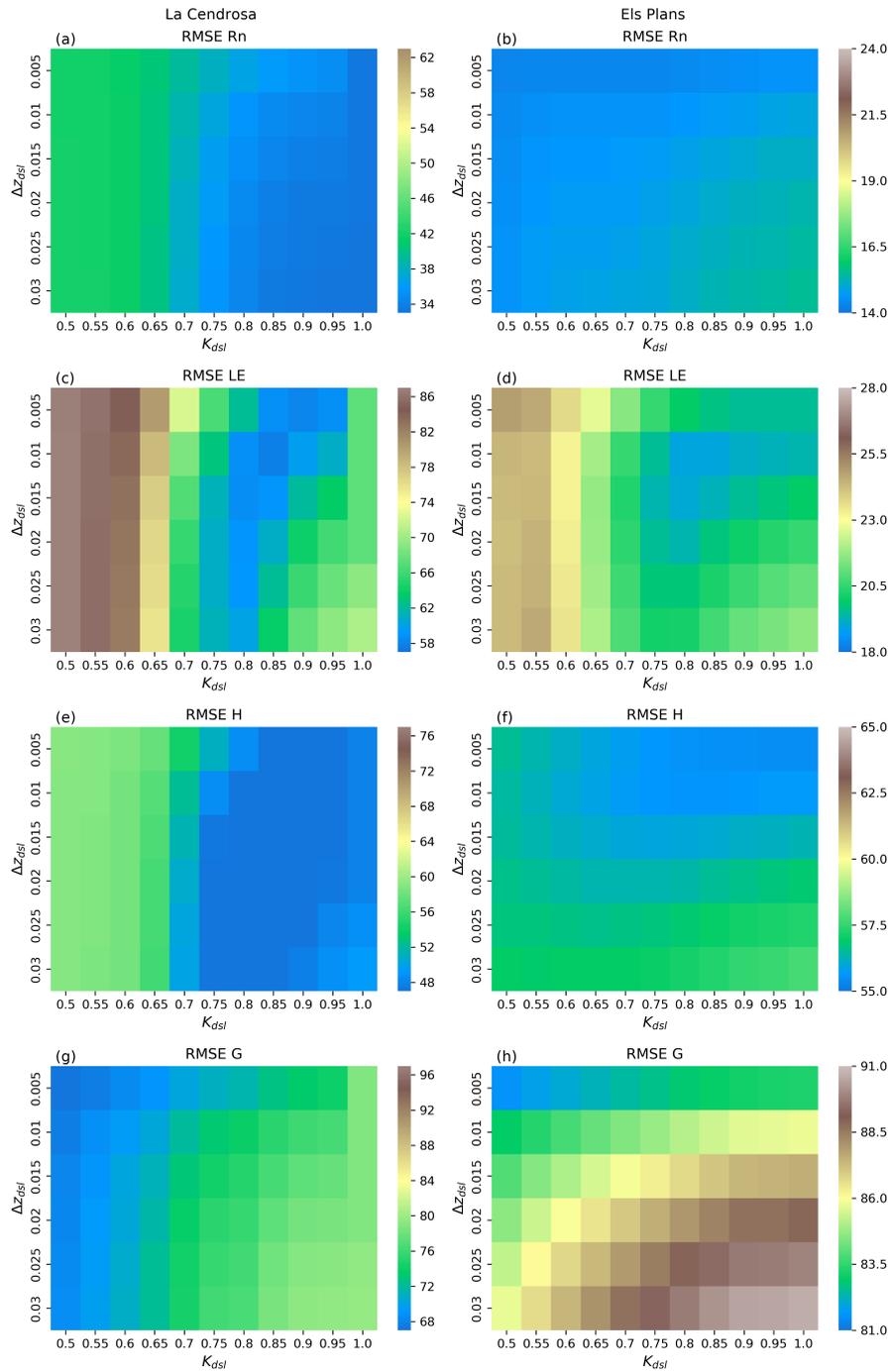
Figure 12. Parameter sensitivity test for the energy budget terms modifying K_{dsl} and z_{dsl} with a DSL resistance for La Cendrosa site [left] and Els Plans [right] during the day. The color represents the resulting RMSE for the daytime for Rn (a), LE (b), H (c), G (d).
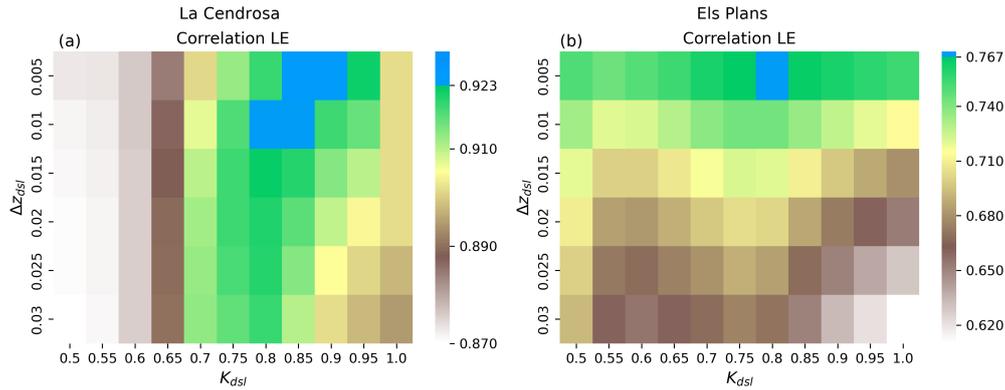
Figure 13. Maps of correlation of LE for La Cendrosa (a) and Els Plans (b).

show the minimum value of RMSE instead of the value found by Swenson and Lawrence (2014). These discrepancies are within what would be expected from the LSM dependence on the characterization of other processes and the use of two
740 contrasting case studies. The error in H is also reduced with a thinner resistance layer. On the other hand, the value of K_{dsl} seems to be optimal at 0.85, closely followed by 0.8, as the error remains within 1 W m^{-2}, which corresponds to the proposed value of Swenson and Lawrence (2014). Zhang et al. (2015) show resistances appearing at values of K_{dsl} close to 0.95 for soils with coarser texture (e.g. higher sand content), but in soils with finer texture, the resistance is first estimated at lower values (0.8 to 0.6). The best values for soils with more clay correspond to values of K_{dsl} of 0.9 or higher, although the resistance has
745 a very small value. A value of K_{dsl} close to 0.8 should allow enough open pore space for a DSL to fully form.

The use of a DSL resistance results in the storage of excess energy in the soil, so that the optimum value for G in ISBA corresponds to the lowest possible soil resistance. Other soil constituents and processes can alter the thermal properties of the soil and are still to be included in LSMs (Vereecken et al. 2019). To improve this flux in SURFEX, a more detailed investigation of the thermal properties of the soil is still needed, but this is outside of the scope of the current study.
750 The correlation values of LE for the values of K_{dsl}=0.8 or 0.85 and $z_{dsl} = 0.1$ m are shown in Fig. 13. The correlation for La Cendrosa is improved over the S92 simulation (daytime in Table 3) and for Els Plans it is equal to or slightly better than the NON simulation (daytime in Table 4). This implies optimal values have a greater resistance than S92 but less than that found in Swenson and Lawrence (2014), for the two sites and specific conditions considered in the current study.

6

755 Estimation of evapotranspiration (ET) in semi-arid environments is continuously improving in LSMs, with ET partitioning being a challenge as there are still few measurements characterizing the components of ET. In this context, two contrasting LIAISE sites were investigated. The default simulations showed an overestimation of ET due to the overestimation of bare soil evaporation, a feature common in multiple LSMs which has been addressed by adding surface resistances of different

forms. As a consequence, a soil resistance has been implemented in SURFEX V9 using two options: Sellers 92, a resistance formulation widely used by LSMs that was incorporated in V8, and a newly implemented DSL resistance that more accurately represents the actual physical process modulating bare-soil evaporation. There was an improvement of almost 30% in RMSE in ET at each site and no degradation of H using the DSL resistance approach. There was an impact on Rn and G which changed mainly due to the increased soil heating owing to reduced LE.

The sites presented several challenges for the model configuration related to vegetation parametrization and management, such as harvesting and irrigation. The first site consisted in an alfalfa field named La Cendrosa, where a detailed characterization of the crop and its biophysical parameters has been made. Such efforts can be later transformed into an informed decision on approximations on a global scale for similar crop types and climates. The development of alfalfa was represented taking into account a daily evolution of LAI and vegetation height based on observations. The study of the photosynthesis parameters used to configure the simulation has shown that the model is sensitive to the cuticular conductance, although it is not the driving mechanism. Instead, the increase in quantum efficiency and the assimilation parameter are most responsible for the increase in ET for alfalfa. It is considered that these measurements and its parameterization in the model improved the estimation of the transpiration. Using a relatively accurate parameter set for photosynthesis and without the presence of the crop after cutting, the DSL resistance becomes important in maintaining the correct amount of bare soil evaporation. The daytime ME and RSME for LE were both reduced by approximately $30\,\mathrm{W\,m^{-2}}$ and the correlation increased from 0.87 to 0.92 when using a DSL, whereas the improvement on H and Rn is of a change in ME and RMSE together of $8\,\mathrm{W\,m^{-2}}$, the same order as the degradation of G.

The second site corresponds to a rain-fed natural dry grassland named Els Plans. An almost continuous DSL resistance together with a very low LAI maintains the very low LE fluxes which is consistent with those observed by the eddy covariance system. The differences for LE in the rate of drying after each rain event point to other processes being involved such as wind speed or air saturation. The DSL resistance produced a similar improvement to the La Cendrosa site, but with a reduction in the correlation of LE. Two factors played a role: the limitations of a low LAI to characterize vegetation at Els Plans site, and a resistance value that does not take into account the internal biases of the ISBA model for both sites, which led to the need for sensitivity tests.

The parameter sensitivity analysis for the DSL resistance approach suggests a slightly lower z_{dsl} value for the two sites used in the current study than that found in Swenson and Lawrence (2014). The correlation of LE increased by 0.01 for La Cendrosa compared to the initial value of z_{dsl}. The correlation with the new values compared to the initial NON simulation was increased by 0.02 at La Cendrosa and is left neutral for Els Plans. The overall error of the simulation was also reduced. The resistance value from the DSL approach was still greater than that obtained when using the S92 method. The point at which resistance begins to develop has been found to be when about twenty percent of the available space in the first layer has been occupied by air.

In addition, the analysis of the two sites has also considered their soil properties, as the DSL involves changes in soil temperature and soil water content. The increase in soil temperature is greater when moisture and bare soil evaporation are significant and the DSL is still present. Laboratory based soil hydraulic properties were available but were found to be

insufficient to reproduce the VWC, a behaviour also reported in Aouade et al. (2020), so it is recommended that further studies include variables that define the soil water retention characteristics when calibrating the model.

795   Finally, the DSL parametrization provides a plausible physical interpretation of the simulated evaporation which is lower than in the baseline scheme while remaining pragmatic since the equation does not represent water vapor transport explicitly. We have shown that it can be applied to conditions that represent the extremes of a semi-arid environment and under different land management practices, including flood irrigation. A multi-site or a global/regional analysis should help to define the choice of parameters for more climates and land cover types. Values with a K_{dsl} between 0.8 and 0.85 and a z_{dsl} near 0.01 m

800   were found for the two sites used in the current study remaining near 0.8 and lower while close to the 0.015 m of Swenson and Lawrence (2014). The DSL resistance methodology seems to be rather robust since similar parameter values are obtained between two different LSMs and varying surface conditions.

Appendix A: Vegetation model description

A1   Components of the vegetation latent heat flux

The components of the vegetation water exchange E_v are given by:

$$E_{tr} = \rho_a \frac{q_{sat,v} - q_c}{R_{avg-c} + R_s}(1 - \delta) \tag{A1}$$

and

$$E_r = \rho_a \frac{q_{sat,v} - q_c}{R_{avg-c}} \delta \tag{A2}$$

with $R_s = 1/g_{sI}$ where g_{sI} is the stomatal conductance at the canopy level and it is the weighted average of the different plant types multiplied by the LAI, ρ_a is the air density, $q_{sat,v}$ is the saturated specific content at the vegetation temperature and q_c is the canopy air specific humidity ($kg kg^{-1}$). R_{avg-c} is the resistance between the overlaying air and vegetation. It consists on the inverse of the sum of the bulk canopy aerodynamic conductance between the canopy and the canopy air (Choudhury and Monteith 1988) and the conductance accounting for the free convection from (Sellers et al. 1986). δ is the Halstead coefficient with a factor to account that saturated vegetation can transpire. See Boone et al. (2017) section 2.6.1 for the particulars of the aerodynamic resistance of the canopy, section 2.8.3 for the Halstead coefficient and their appendix C2 for the LE formulation, which fall outside the discussions of this article.

A2   A-gs model

A2.1   Transpiration formulation

The A-gs (Assimilation-stomatal conductance) scheme of Goudriaan et al. (1985) within SURFEX presents the parametrization of plant assimilation of carbon. It was modified by Jacobs et al. (1996) to model photosynthesis and it can be used to obtain transpiration. Different types of vegetation can be selected and its parametrizations are modeled as a function of the so-called vegetation patch (or land cover type). In SURFEX, a patch corresponds to a Plant Functional type (PFT), which characterizes subcategories natural land-surfaces. Additionally, vegetation can have either drought tolerant or drought avoidant strategies (Calvet et al. 2004). A description of the processes can be found in Calvet et al. (1998) and Delire et al. (2020).

In order to describe the parameter selection methodology, we provide the mathematical development of the low vegetation scheme in ISBA (Calvet 2000), which is used to represent crops and herbaceous types in contrast to high vegetation that considers woody types. The main difference is in the relationship between the mesophilic conductance and the maximum humidity deficit. A glossary containing the parameter definitions is provided in Appendix D. Transpiration in A-gs is given by:

$$E_T = \rho_a g_s D_s \tag{A3}$$

D_s is the specific humidity deficit. D_s indicates when stomata are closed by exceeding D_{max}, the maximum specific humidity deficit of the air tolerated by the vegetation (with no soil water stress). The stomatal conductance calculation is presented in Appendix A3 for thoroughness. D_s is of the form:

$$D_s = \frac{f - f_0^*}{f_{min} - f_0^*} D_{max} \tag{A4}$$

where f indicates the proportionality of internal CO_2 inside the leaf boundary layer and f_0^* is f with no saturation deficit (without soil water stress) and are model parameters (see Table A1). f_{min} is the minimal value of f:

$$f_{min} = \frac{g_c}{g_c + g_m^*} \tag{A5}$$

where g_m^* is the mesophyllic conductance and g_c is the cuticular conductance. g_m^* determines the gas exchange amount through the stomata and g_c through the cuticle when stomata are completely closed, they depend on the plant type rather than on C3/C4 strategy. The cuticle is a kind of wax membrane that protects the leaf and allows little exchange of gases, its values being smaller than those of g_m^*. Both contribute to the total transpiration.

A2.2 Evaporation strategies

D_{max} behavior varies with evaporation strategy, limiting transpiration depending on its value. The formulation is the following:

$$D_{max} = D_{max}^+ + (D_{max}^* - D_{max}^+) \frac{f_2 - f_{2c}}{1 - f_{2c}} \tag{A6}$$

where D_{max}^+ can be N for the drought-avoiding strategy applied for C3 crops (eq. A7), and X for the drought-tolerant strategy (eq. A9). Given the same D_{max}, transpiration will decrease for C3 and increase for C4 plants under water stress conditions due to these different strategies. For C3 crops D_{max}^* is given by:

$$\ln(g_m^*) = 2.381 - 0.6103 \ln(D_{max}^*) \tag{A7}$$

and

$$f_2 = \sum_{i=1}^{Ng} \zeta_i \frac{\omega_{g,i} - \omega_{wilt,i}}{\omega_{fc,i} - \omega_{wilt,i}} \tag{A8}$$

where f_2 is the normalized soil moisture and f_{2c} is its tabulated critical value. f_2 is summed over the soil layers Ng (Decharme et al. 2011). Soil water content variables are represented by ω. The first subindex indicates the water content variable, g is the ground, $wilt$ is the wilting point and fc is the field capacity. The second subindex corresponds to the layer number to which it pertains, 1 would indicate the most superficial layer. ζ_i represents the difference in the cumulative root zone fraction for a given layer. Within this strategy D_{max} increases until critical soil moisture is reached ($f_2 = f_{2c}$), then the previous g_m^* symbolized by g_m^{*X} is updated and decreases with the water deficit: $g_m^* = g_m^{*X} f_2 / f_{2c}$.

Table A1. Table of default parametrized values in the A-gs scheme for the used PFT.

	f	f_0^*	D_{max}^N	D_{max}^X	f_{2c}	$Q_{10}(25)$	$T_1(g_m^*, A_{m,max})$	$T_2(g_m^*, A_{m,max})$
units	-	-	$g\,kg^{-1}$	$g\,kg^{-1}$	-	-	$°C$	$°C$
C3 crop/herbaceous	6.73	0.25	30	300	0.3	2.0	5,13	36,36
C4 crop/herbaceous	-4.33	0.15	30	300	0.3	2.0	8,13	38,38

For the drought tolerant strategy used for C4 crops and in our simulated alfalfa, we take Eq. (A6), with D_{max}^* given by:

$$\ln(g_m^*) = 5.323 - 0.8923 \ln(D_{max}^*) \tag{A9}$$

In this strategy then D_{max} increases until the critical soil moisture is reached, D_{max} decreases with the severity of the stress: $D_{max} = D_{max}^X f_2 / f_{2c}$. Note that this is the opposite behavior from C3 crops as D_{max}^* and g_m^* are anticorrelated. The calculation of g_s is included in Appendix A3 for thoroughness and to facilitate the interpretation of LE changes: a glossary has been included at the end of the document in Appendix D1.

A3   Stomatal conductance

To obtain g_s we use the following expressions:

$$g_s = 1.6 g_{sc} + g_c \tag{A10}$$

where g_{sc} is the stomatal conductance to CO_2 given by:

$$g_{sc} = g_{sc}^{first} + E^{first} \frac{M_a}{\rho_a M_v} \frac{C_s + C_i}{2(C_s - C_i)} \tag{A11}$$

where M_a and M_v are molecular masses of air and water vapor respectively, C_s is the external concentration of CO_2 and C_i the CO_2 internal concentration, expressed as:

$$C_i = f C_s + (1 + f)\Gamma \tag{A12}$$

and

$$\Gamma(T_s) = \Gamma(25) Q_{10}^{T_s - 25}/10 \tag{A13}$$

where Γ is the CO_2 compensation concentration at the skin temperature, T_s is the superficial temperature of the leaf and Q_{10} is fixed at 2.0 (see Table A1).

To obtain E^{first} with equation (A3), $g_s^{first} = 1.6 g_{sc}^{first}$ accounting for the ratio of CO_2 to water assimilation for the stomatal conductance to CO_2 with:

$$g_{sc}^{first} = \frac{A_n - A_{min}\left[\frac{D_s}{D_{max}^*}\left(\frac{A_n + R_d}{A_m + R_d}\right) + R_d\left(1 - \frac{A_n + R_d}{A_m + R_d}\right)\right]}{C_s - C_i} \tag{A14}$$

where $R_d = A_m/9$ and corresponds to the dark respiration. A_m is the CO_2 assimilation limited by the air CO_2 concentration due to saturation, and A_n is the CO_2 assimilation limited by the air CO_2 concentration. A_{min} represents the residual photosynthesis rate (at full light intensity) associated with cuticular transfers when the stomata are closed because of a high specific humidity deficit, it is expressed as:

$$A_{min} = g_m^*(C_{min}\Gamma) \tag{A15}$$

where C_{min} is the minimum value of C_i at D_{max}^*, given by:

$$C_{min} = \frac{g_c C_s + g_m^* \Gamma}{g_c + g_m^*} \tag{A16}$$

Additionally, A_m is:

$$A_m = A_{m,max}\left(1 - \exp\frac{-g_m^*(C_i - \Gamma)}{A_{m,max}}\right) \tag{A17}$$

with:

$$A_{m,max} = \frac{A_{m,max}(25)Q_{10}^{(Ts-25)/10}}{(1 + \exp[0.3(T_1 - T_s)])(1 + \exp[0.3(T_s - T_2)])} \tag{A18}$$

with T_1 and T_2 being reference temperature values.

$$A_n = (A_m + R_d)\left(1 - \exp\left(\frac{-\epsilon I_a}{A_m + R_d}\right)\right) - R_d \tag{A19}$$

where I_a is the photosynthetically active radiation and

$$\epsilon = \epsilon_0\left(\frac{C_i - \Gamma}{C_i + 2\Gamma}\right) \tag{A20}$$

where ϵ_0 is the quantum efficiency.

The relationships from (A3) to (A20) show that g_s is highly nonlinear with the parameters g_m^*, g_c, $A_{m,max}(25)$ and ϵ_0. D_s is in fact $D_s(g_m^*, g_c)$ and $A_n = A_n(g_m^*, g_c, \epsilon_0, A_{max})$ between others. Discussion on the values of these parameters is done in Sect. 4.2.1 and in further detail Appendix B1.

Appendix B: Detailed model configuration

B1 Vegetation parameterization of alfalfa

A realistic transpiration simulation is essential for obtaining a good estimate of LE, particularly for alfalfa. The process is governed by several parameters that are best prescribed from observational data when available (see Sect. 3.2). We explore them

with the AST option within SURFEX in all simulation configurations. With this option, the A-gs scheme is employed to model photosynthesis, parameterizing its processes, in contrast to other options that model transpiration directly without considering the biological processes. The vegetation can exhibit either drought-tolerant, Eq. (A9), or drought-avoidant strategies, Eq. (A7) (Calvet et al. 2004), previously described in Appendix A2.2. The A-gs scheme is rarely compared with direct vegetation measurements (Van Diepen et al. 2022) due to the difficulty of achieving a one-to-one correspondence for the model parameters. Direct observations of stomatal conductance (g_s), CO2 assimilation and photosynthetically active radiation (PAR) were obtained at La Cendrosa. The mesophylic (g_m^*) and cuticular conductances (g_c), and the maximum assimilation ($A_{m,max}(25)$) can be found from observations or via the maximum catalytic capacity of Rubisco (V_{cmax}), the enzyme that controls energy production. In contrast, quantum efficiency (ϵ_0) is usually a fitted parameter when the energy, assimilation and carbon curves are measured. After testing multiple parameter configurations, it was found that increasing the quantum efficiency, ϵ_0, and the maximum assimilation ($A_{m,max}(25)$) gave results that reproduce results obtained with a higher cuticular conductance. More energy than the default must be supplied to match the observed fluxes, regardless of whether it comes from the stomata or the cuticle. For this reason, the model adaptations are described below.

– Mesophyll conductance: The PFT parametrization establishes the g_m^* through an associated curve that varies depending on whether the water use efficiency strategy under moderate stress is stress tolerant, Eq. (A9), or stress avoidant, Eq. (A7), and only one type is associated with each vegetation type (Calvet 2000). Although alfalfa is a C3 crop, its drought strategy is tolerant as in C4 crops. Such plants species are known as C4-like species (Way et al. 2014). In consequence, the stress type has been changed to drought tolerant for the simulation. For this site, the highest impact comes from the increase in absolute transpiration and not from the possible changes in stomata closure. With this strategy, parameters are set for generic species and must be modified to represent a particular species. The g_m^* values have been changed to $0.005\,m\,s^{-1}$ (see Table B1). These values are within the observed values of the control (Aranjuelo et al. 2013) and lower values would correspond to stressed alfalfa. Lower values of $0.00197\,m\,s^{-1}$ were also observed with unstressed alfalfa (Malik et al. 2018). For the CLASS model (De Arellano et al. 2015), González-Armas et al. (2023) used a g_m^* value of $0.01\,m\,s^{-1}$ which was found for the same site. After setting the other parameters, the differences in mean error and root mean square error modifying the g_m^* value from 0.005 to $0.1\,m\,s^{-1}$ in SURFEX are below $1\,W\,m^{-2}$ for all fluxes. Differences arise on the days on which stomatal closure is simulated and depend on what degree the closure is effective. It should be noted that alfalfa is bred for the development of drought/salinity tolerant varieties that are thus optimized for cultivation in arid and semi-arid regions of the Mediterranean area (Mouradi et al. 2022). However, the modification of this parameter is necessary, but there are still errors in the estimation of ET so additional parameters are explored.

– Cuticular conductance: As a first approximation, increasing the cuticular conductance to $0.0006\,m\,s^{-1}$ provided good estimates of ET. Measurements of cuticular conductance can follow several strategies and give different values for the same species (Kerstiens 1996). Simplification to a minimum value of conductance ($gmin$) and other similar values such as nocturnal conductance or detached leaf conductance are more commonly measured (Duursma et al. 2019), $gmin$ values are more similar to values of g_c which serve as a default in numerical simulations and are used as a proxy. For

alfalfa, the value was set to $0.00007\,m\,s^{-1}$ according to Kerstiens (1996). When used, it provided simulations with a profound dip in evaporation in the central part of the day, resulting in unrealistic results compared to observations. No further values of g_c for alfalfa were found in the literature, which could probably indicate the difficulty of measuring this parameter. The Kerstiens (1996) value is one order of magnitude below the tested value of $0.0006\,m\,s^{-1}$ and three times less than the default value in SURFEX of $0.00025\,m\,s^{-1}$. The default value has been used as it is closer to the literature value without being outside the typical observed values of this parameter for other vegetation. Values up to at least $0.006\,m\,s^{-1}$ can still provide reasonable estimations of ET but are outside the reported values and they are non-physical. This behavior is given by the relationships from equations (A16) and (A5), which holds the sum of g_c and g_m^* in the denominator and can compensate the effects from one another. Together with Eq. (A10), an increase of g_c produces a similar effect to increasing g_m^*.

– Quantum efficiency: The ϵ_0 can be directly related to the increase in transpiration, an increase of ϵ_0 in Eq. (A20) induce an increase in carbon assimilation in Eq. (A19) and of the stomatal conductance, Eq. (A10). This parameter is based on the theoretical quantum requirement of photons needed to assimilate one molecule of CO_2 (Von Caemmerer and Farquhar 1981) , and it limits the assimilation rate (see review in Van Diepen et al. (2022)). Goudriaan et al. (1985) presents a revised value of $0.017\,\mathrm{mg}\,CO_2\,\mathrm{J}^{-1}$ and suggests that selective breeding of the plant species could lead to an increase in this value in new varieties. Its value has not evolved in the SURFEX configuration over the years. There is some evidence that this value is variable; Collatz et al. (1992) showed a small temperature dependence and Cai and Dang (2002) identified a variability of this parameter within tree species, but the exploration of this parameter in measurements has seemingly not progressed in recent years for meteorological applications. Mouradi et al. (2022) and Jiang et al. (2009) show that depending on the alfalfa variety, the electron transport rate and the PAR conversion efficiency (biological measurements used by their community) can be increased, apparently exploiting an increase in electron efficiency, although no direct conversion to these parameters has been found. This efficiency will decrease during drought events (Zhang et al. 2019; Mouradi et al. . Thus, the ϵ_0 value used may be more variable than reported and may have been compensated by an increase in other parameters such as cuticular conductance. The ϵ_0 value of $0.0265\,\mathrm{mg}\,CO_2\,\mathrm{J}^{-1}$ found by González-Armas et al. (2023) increases the LE to values closer to the observed values and is therefore used in this study.

– Maximum assimilation: The $A_{m,max}(25)$ sensitivity is most relevant for low LAI values, as marginal increases of this value will be weighted more heavily to increase transpiration than for other parameters. The relationship of $A_{m,max}$ in Eq. A14 has a nonlinear response for g_s. The increase of $A_{m,max}(25)$ in Eq. (A18) increases A_n in Eq. (A19) and on to the stomatal conductance, Eq. (A10), but $A_{m,max}$ can also be found in the denominator.

The default value of $A_{m,max}(25)$ is $2.2\,\mathrm{mg}$. For alfalfa, both higher values (Bunce 2018) with $2.64\,\mathrm{mg}$, which were transformed from V_{cmax} as in Collatz et al. (1991), and lower values (Malik et al. 2018) of $1.4\,\mathrm{mg}$ have been reported in the literature. González-Armas et al. (2023) found values ($3.02\,\mathrm{mg}$) at La Cendrosa that were considerably higher than those given in the literature and the standard value in SURFEX. Increasing this value in this simulation improves

Table B1. Values for alfalfa of the tested variables of the A-gs configuration in SURFEX. The simulated value corresponds to the final set of parameters used in the results section.

Variable	symbol	units	default value	simulated value	tested range	literature range
Mesophylic conductance	g_m^*	$\mathrm{m\,s^{-1}}$	0.001	0.005	0.0005-0.2	0.002-0.01
Cuticular conductance	g_c	$\mathrm{m\,s^{-1}}$	0.00025	0.00025	0.00007-0.006	0.00007
Quantum efficiency	ϵ_0	$\mathrm{mg\,J^{-1}}$	0.017	0.0265	0.017-0.0265	0.017-0.0265
Maximum assimilation	$A_{m,max}(25)$	$\mathrm{mg\,m^{-2}s^{-1}}$	2.2	3.02	1.4-3.02	1.4-3.02

the transpiration estimates for days that show a dip in ET during the day reducing its intensity, therefore the value in González-Armas et al. (2023) is kept, but the default values are adequate for most of the simulated days.

Appendix C: Further model components

C1 Ground heat flux

990 The energy budget equation on the SURFEX model can be written as:

$$Rn - H - LE - G' - S = 0 \tag{C1}$$

where S is the energy storage term and G' the conduction flux given a particular ground level. G is given then by G' - S and it is defined at the surface.

44

Appendix D: Variable and parameter glossary

Table D1: Glossary table with the variables presented in the article.*Indicates that the variable is linked to the equation text. **The equations are in ppm but the SURFEX input is in kg m^{-3}

parameter	symbol	units	Equation/Table
Net radiation	Rn	W m^{-2}	-
Latent heat flux	LE	W m^{-2}	eq. (1)
Sensible heat flux	H	W m^{-2}	-
Ground heat flux	G	W m^{-2}	-
Accumulated latent heat flux	E	mm	-
Leaf area index	LAI	$\text{m}^2\,\text{m}^{-2}$	Table 1
Heat of vaporization	L_v	J kg^{-1}	eq. (1)
Evaporation	E_v	$\text{kg m}^{-2}\,\text{s}^{-1}$	eq. (1)
Soil evaporation	E_g	$\text{kg m}^{-2}\,\text{s}^{-1}$	eq. (1), (2)
Plant transpiration	E_{tr}	$\text{kg m}^{-2}\,\text{s}^{-1}$	eq. (A1)
Canopy intercepted liquid water evaporation	E_r	$\text{kg m}^{-2}\,\text{s}^{-1}$	eq. (A2)
Air density	ρ_a	kg m^{-3}	eq. (A1),(A2),(A3), (2)
Saturated specific humidity	$q_{sat,v}$	kg kg^{-1}	eq. (A1), (A2)
Ground specific humidity	$q_{sat,g}$	kg kg^{-1}	eq. (2)
Canopy air specific humidity	q_c	kg kg^{-1}	eq. (A1), (A2), (2)
LAI-weighted stomatal conductance	g_{sI}	m s^{-1}	eq. (A1)
Air to vegetation resistance	R_{avg-c}	s m^{-1}	eq. (A1), (A2)
Air to ground resistance	R_{ag}	s m^{-1}	eq. (2)
Stomatal resistance	R_s	s m^{-1}	eq. (A1)
Soil resistance	R_{soil}	s m^{-1}	eq. (2), (4), (5)
Halstead coefficient	δ	-	eq. (A1), (A2)
Carbon dioxide	CO_2	ppm**	-
Air molecular mass	M_a	g mol^{-1}	eq. (A11)
Water vapor molecular mass	M_v	g mol^{-1}	eq. (A11)
Transpiration (A-gs)	E_T	$\text{kg m}^{-2}\,\text{s}^{-1}$	eq. (A3)
Transpiration initial value	E^{first}	$\text{kg m}^{-2}\,\text{s}^{-1}$	eq. (A11)
stomatal conductance	g_s	m s^{-1}	eq. (A3), (A10)
Stomatal conductance to CO_2	g_{sc}	m s^{-1}	eq. (A10), (A11)
g_{sc} initial value	g_{sc}^{first}	m s^{-1}	eq. (A11), (A14)

g_s initial value	g_s^{first}	m s^{-1}	eq. (A14)*
Mesophyllic conductance	g_m^*	m s^{-1}	eq. (A5), (A7), (A9), (A15), (A16), (A17)
Previous step mesophyllic conductance	g_m^{*X}	m s^{-1}	eq. (A7)*
Cuticular conductance	g_c	m s^{-1}	eq. (A5), (A16)
Specific humidity deficit	D_s	g kg^{-1}	eq. (A3), (A4)
Maximum specific humidity deficit	D_{max}	g kg^{-1}	eq. (A4), (A6)
Default initial D_{max}	D_{max}^+	g Kg^{-1}	eq. (A6)
C3 default initial D_{max}	D_{max}^N	g Kg^{-1}	eq. (A6)*, Table A1
C4 default initial D_{max}	D_{max}^X	g Kg^{-1}	eq. (A6)*, Table A1
Strategy-dependent D_{max}	D_{max}^*	g Kg^{-1}	eq. (A6), (A7), (A9)
CO_2 proportionality between leaf inside and its boundary layer	f	-	eq. (A4), (A12)
f minimal value	f_{min}	-	eq. (A4), (A5)
f under no soil water stress	f_0^*	-	eq. (A4)
Normalized soil moisture	f_2	m^{3}m^{-3}	eq. (A6), (A8)
Critical normalized soil moisture	f_{2c}	m^{3}m^{-3}	eq. (A6)
Soil water content at layer i	ω_i	m^{3}m^{-3}	-
ω_i at layer i wilting point	$\omega_{wilt,i}$	m^{3}m^{-3}	eq. (A8)
ω_i at layer i field capacity	$\omega_{fc,i}$	m^{3}m^{-3}	eq. (A8), (3)
ω_i at ground layer i	$\omega_{g,i}$	m^{3}m^{-3}	eq. (A8), (3)
ω_i at a saturated value	$\omega_{sat,i}$	m^{3}m^{-3}	eq. (4), (3), (6)
Cummulative root zone fraction at layer i	ζ_i	-	eq. (A8)
Soil humidity coefficient	h_y	-	eq. (3)
Maximum DSL thickness	ΔDSL	m	eq. (5)
DSL activation water content	ω_{dsl0}	m^{3}m^{-3}	eq. (5)
Air dry soil moisture	ω_{air}	m^{3}m^{-3}	eq. (5)
Porosity	Φ	m^{3}m^{-3}	eq. (9)
Air-filled pore space	Φ_{air}	m^{3}m^{-3}	eq. (9)
Proportionality porosity coefficient	K_{dsl}	-	eq. (5)
Air dry matric potential	Ψ_{air}	m	eq. (6)
Water saturated matric potential	Ψ_{sat}	m	eq. (6), Table 2
Saturated hydraulic conductivity	K_{sat}	-	Table 2
Slope of water retention curve	b	-	eq. (6)
Tortuosity of vapor flow paths	τ_v	m^{3}m^{-3}	eqs. (7), (9)
Molecular diffusivity of water vapor flow	D_{va}	m^2 s^{-1}	eq. (8)

Standard reference pressure	p_0	Pa	eq. (8)
Air pressure	p	Pa	eq. (8)
Soil temperature at first level	$T_{g,1}$	K	eq. (8)
Freezing temperature to water	T_f	K	eq. (8)
Roughness length	z_0	m	Table 1
Heat roughness length	z_{oh}	m	Table 1
Vegetation height	H_{veg}	m	Table 1
Soil depth	d	m	Table 2
External concentration of CO_2	C_s	ppm**	eq. (A11), (A12), (A14), (A16)
Leaf internal concentration of CO_2	C_i	ppm**	eq. (A11), (A12), (A14), (A16), (A17), (A20)
Minimal value of C_i at D^*_{max}	C_{min}	ppm**	eq. (A15), (A16)
Skin temperature	T_s	K	eq. (A13), (A18)
Lower reference temperature	T_1	K	eq. (A18)
Higher reference temperature	T_2	K	eq. (A18)
CO_2 compensation concentration			
at skin temperature	Γ	ppm	eq. (A13), (A12), eq. (A15), (A17)
CO_2 compensation coefficient	Q_{10}	-	eq. (A13), (A12)
Dark respiration	R_d	mg m^{-2} s^{-1}	eq. (A14), (A19)
CO_2 assimilation limited by CO_2 saturated air	A_m	mg m^{-2} s^{-1}	eq. (A14), (A17), (A19)
Maximal value of A_m	$A_{m,max}$	mg m^{-2} s^{-1}	eq. (A17), (A18)
Maximum assimilation value at 25°C	$A_{m,max}(25)$	mg m^{-2} s^{-1}	eq. (A18), Table B1
CO_2 assimilation limited by			
air CO_2 concentration	A_n	mg m^{-2} s^{-1}	eq. (A14), (A19)
Residual photosynthesis rate	A_{min}	mg m^{-2} s^{-1}	eq. (A14), (A15)
Quantum efficiency	ϵ_0	mg J^{-1}	eq. (A20), Table B1
Initial quantum use efficiency	ϵ	mg J^{-1}	eq. (A19), (A20)
Photosynthetically active radiation	I_a	W m^{-2}	eq. (A19)

995 **Appendix E: Sensors**

Table E1. Instruments at the selected SEB stations (N.A. represents non-applicable). CSAT3, EC150 and Krypton are Campbell Scientific (CS) Instruments; LI stands for LI-COR, HS-50 and R3-50 are Gill models, CNR1, CNR4, CRg4 and CM21 are Kipp & Zonen devices, the flux plates are made by Hukseflux. There were two SEB stations at La Cendrosa from the CNRM and from WUR.

Site	Sonic and gas analyzer height (m)	Net radiation, height (m)	Flux plate depth (cm)	Soil temperature: depths (cm)	soil moisture depths(cm)
La Cendrosa	Gill R3-50, LI7550, 3.0	CNR4, 1.0	3	Generic Pt100, 5, 10, 30	Delta T Thetaprobe ML3, 5, 10, 30
La Cendrosa	IRGASON, LiCor7500, 1.0	CM11 & CG2	5	Generic Pt100, 2, 10	N.A.
Els Plans	HS-50, Krypton, 2.0	CRg4/ CM21, 1.0	2	Delta T ST2 1, 4, 10, 17, 35, 50	Delta T ML3, 10, 20, 30, 40

References

Al-Yemeni, M. N. and Grace, J.: Radiation balance of an alfalfa crop in Saudi Arabia, Journal of Arid Environments, 29, 447–454, 1995.

Alton, P., Fisher, R., Los, S., and Williams, M.: Simulations of global evapotranspiration using semiempirical and mechanistic schemes of plant hydrology, Global Biogeochemical Cycles, 23, 2009.

Aouade, G., Jarlan, L., Ezzahar, J., Er-Raki, S., Napoly, A., Benkaddour, A., Khabba, S., Boulet, G., Garrigues, S., Chehbouni, A., et al.: Evapotranspiration partition using the multiple energy balance version of the ISBA-Ag s land surface model over two irrigated crops in a semi-arid Mediterranean region (Marrakech, Morocco), Hydrology and Earth System Sciences, 24, 3789–3814, 2020.

Aranjuelo, I., Tcherkez, G., Molero, G., Gilard, F., Avice, J.-C., and Nogués, S.: Concerted changes in N and C primary metabolism in alfalfa (Medicago sativa) under water restriction, Journal of experimental botany, 64, 1–17, 2013.

Aubinet, M., Grelle, A., Ibrom, A., Rannik, Ü., Moncrieff, J., Foken, T., Kowalski, A. S., Martin, P. H., Berbigier, P., Bernhofer, C., et al.: Estimates of the annual net carbon and water exchange of forests: the EUROFLUX methodology, in: Advances in ecological research, vol. 30, pp. 113–175, Elsevier, 2000.

Balugani, E., Lubczynski, M., Van Der Tol, C., and Metselaar, K.: Testing three approaches to estimate soil evaporation through a dry soil layer in a semi-arid area, Journal of hydrology, 567, 405–419, 2018.

Balugani, E., Lubczynski, M., and Metselaar, K.: Evaporation through a dry soil layer: Column experiments, Water Resources Research, 57, e2020WR028 286, 2021.

Balugani, E., Lubczynski, M., and Metselaar, K.: Lysimeter and in situ field experiments to study soil evaporation through a dry soil layer under semi-arid climate, Water Resources Research, 59, e2022WR033 878, 2023.

Barr, A. G., King, K., Gillespie, T., Den Hartog, G., and Neumann, H.: A comparison of Bowen ratio and eddy correlation sensible and latent heat flux measurements above deciduous forest, Boundary-Layer Meteorology, 71, 21–41, 1994.

Barton, I.: A parameterization of the evaporation from nonsaturated surfaces, Journal of Applied Meteorology (1962-1982), pp. 43–47, 1979.

Bell, L. W., Williams, A. H., Ryan, M. H., and Ewing, M. A.: Water relations and adaptations to increasing water deficit in three perennial legumes, Medicago sativa, Dorycnium hirsutum and Dorycnium rectum, Plant and soil, 290, 231–243, 2007.

Best, M. J., Pryor, M., Clark, D., Rooney, G. G., Essery, R., Ménard, C., Edwards, J., Hendry, M., Porson, A., Gedney, N., et al.: The Joint UK Land Environment Simulator (JULES), model description–Part 1: energy and water fluxes, Geoscientific Model Development, 4, 677–699, 2011.

Béziat, P., Rivalland, V., Tallec, T., Jarosz, N., Boulet, G., Gentine, P., and Ceschia, E.: Evaluation of a simple approach for crop evapotranspiration partitioning and analysis of the water budget distribution for several crop species, Agricultural and Forest Meteorology, 177, 46–56, 2013.

Boone, A., Samuelsson, P., Gollvik, S., Napoly, A., Jarlan, L., Brun, E., and Decharme, B.: The interactions between soil–biosphere–atmosphere land surface model with a multi-energy balance (ISBA-MEB) option in SURFEXv8–Part 1: Model description, Geoscientific Model Development, 10, 843–872, 2017.

Boone, A., Bellvert, J., Best, M., Brooke, J. K., Canut-Rocafort, G., Cuxart, J., Hartogensis, O., Le Moigne, P., Miró, J. R., Polcher, J., Price, J., Quintana Seguí, P., Bech, J., Bezombes, Y., Branch, O., Cristóbal, J., Dassas, K., Fanise, P., Gibert, F., Goulas, Y., Groh, J., Hanus, J., Hmimina, G., Jarlan, L., Kim, E., Le Dantec, V., Le Page, M., Lohou, F., Lothon, M., Mangan, M. R., Martí, B., Martínez-Villagrasa, D., McGregor, J., Kerr-Munslow, A., Ouaadi, N., Philibert, A., Quiros-Vargas, J., Rascher, U., Siegmann, B., Udina, M., Vial, A., Wrenger,

B., Wulfmeyer, V., and Zribi, M.: The Land Surface Interactions with the Atmosphere over the Iberian Semi-Arid Environment (LIAISE) Field Campaign, Journal of the European Meteorological Society, 2, 100 007, 2025.

Brooke, J.: LIAISE_ELS-PLANS_UKMO_LAI_01DAY_L1 [Dataset] Aeris, https://doi.org/10.25326/522, 2023.

1035 Brooke, J., Best, M., Lock, A., Osborne, S., Price, J., Cuxart, J., Boone, A., Canut-Rocafort, G., Hartogensis, O., and Roy, A.: Irrigation contrasts through the morning transition, Quarterly Journal of the Royal Meteorological Society, 2023.

Brut, A., Rüdiger, C., Lafont, S., Roujean, J.-L., Calvet, J.-C., Jarlan, L., Gibelin, A.-L., Albergel, C., Le Moigne, P., Soussana, J.-F., et al.: Modelling LAI at a regional scale with ISBA-A-gs: comparison with satellite-derived LAI over southwestern France, Biogeosciences, 6, 1389–1404, 2009.

1040 Brutsaert, W.: On a derivable formula for long-wave radiation from clear skies, Water resources research, 11, 742–744, 1975.

Bunce, J.: Thermal acclimation of the temperature dependence of the V Cmax of Rubisco in quinoa, Photosynthetica, 56, 1171–1176, 2018.

Cai, T. and Dang, Q.-L.: Effects of soil temperature on parameters of a coupled photosynthesis–stomatal conductance model, Tree Physiology, 22, 819–828, 2002.

Calvet, J.-C.: Investigating soil and atmospheric plant water stress using physiological and micrometeorological data, Agricultural and Forest
1045 Meteorology, 103, 229–247, 2000.

Calvet, J.-C., Noilhan, J., Roujean, J.-L., Bessemoulin, P., Cabelguenne, M., Olioso, A., and Wigneron, J.-P.: An interactive vegetation SVAT model tested against data from six contrasting sites, Agricultural and Forest Meteorology, 92, 73–95, 1998.

Calvet, J.-C., Rivalland, V., Picon-Cochard, C., and Guehl, J.-M.: Modelling forest transpiration and CO2 fluxes—Response to soil moisture stress, Agricultural and forest meteorology, 124, 143–156, 2004.

1050 Camillo, P. J. and Gurney, R. J.: A resistance parameter for bare-soil evaporation models, Soil Science, 141, 95–105, 1986.

Canut, G.: LIAISE_LA-CENDROSA_CNRM_MTO-FLUX-30MIN$_{L2}$ [Dataset] Aeris, https://doi.org/10.25326/320, 2022a.

Canut, G.: LIAISE_PREIXANA_CNRM_MTO-FLUX-30MIN$_{L2}$ [Dataset] Aeris, https://doi.org/10.25326/361, 2022b.

Chang, L.-L., Dwivedi, R., Knowles, J. F., Fang, Y.-H., Niu, G.-Y., Pelletier, J. D., Rasmussen, C., Durcik, M., Barron-Gafford, G. A., and Meixner, T.: Why do large-scale land surface models produce a low ratio of transpiration to evapotranspiration?, Journal of Geophysical Research: Atmospheres, 123, 9109–9130, 2018.

Chanzy, A., Mumen, M., and Richard, G.: Accuracy of top soil moisture simulation using a mechanistic model with limited soil characterization,
1055 Water resources research, 44, 2008.

Choudhury, B. J. and Monteith, J.: A four-layer model for the heat budget of homogeneous land surfaces, Quarterly Journal of the Royal Meteorological Society, 114, 373–398, 1988.

Clapp, R. B. and Hornberger, G. M.: Empirical equations for some soil hydraulic properties, Water resources research, 14, 601–604, 1978.

Coenders-Gerrits, A., Van der Ent, R., Bogaard, T., Wang-Erlandsson, L., Hrachowitz, M., and Savenije, H.: Uncertainties in transpiration
1060 estimates, Nature, 506, E1–E2, 2014.

Collatz, G. J., Ball, J. T., Grivet, C., and Berry, J. A.: Physiological and environmental regulation of stomatal conductance, photosynthesis and transpiration: a model that includes a laminar boundary layer, Agricultural and Forest meteorology, 54, 107–136, 1991.

Collatz, G. J., Ribas-Carbo, M., and Berry, J. A.: Coupled photosynthesis-stomatal conductance model for leaves of C4 plants, Functional Plant Biology, 19, 519–538, 1992.

1065 Coudert, B., Ottlé, C., Boudevillain, B., Demarty, J., and Guillevic, P.: Contribution of thermal infrared remote sensing data in multiobjective calibration of a dual-source SVAT model, Journal of Hydrometeorology, 7, 404–420, 2006.

Cuntz, M., Mai, J., Samaniego, L., Clark, M., Wulfmeyer, V., Branch, O., Attinger, S., and Thober, S.: The impact of standard and hard-coded parameters on the hydrologic fluxes in the Noah-MP land surface model, Journal of Geophysical Research: Atmospheres, 121, 10–676, 2016.

Cuxart, J., Conangla, L., and Jiménez, M.: Evaluation of the surface energy budget equation with experimental data and the ECMWF model in

1070   the Ebro Valley, Journal of geophysical research: atmospheres, 120, 1008–1022, 2015.

Dare-Idowu, O., Jarlan, L., Le-Dantec, V., Rivalland, V., Ceschia, E., Boone, A., and Brut, A.: Hydrological Functioning of maize crops in Southwest France using eddy covariance measurements and a land surface model, Water, 13, 1481, 2021.

De Arellano, J. V.-G., van Heerwaarden, C. C., van Stratum, B. J., and van den Dries, K.: Atmospheric boundary layer: Integrating air chemistry and land interactions, Cambridge University Press, 2015.

1075 De Silans, A. P., Bruckler, L., Thony, J., and Vauclin, M.: Numerical modeling of coupled heat and water flows during drying in a stratified bare soil—comparison with field observations, Journal of Hydrology, 105, 109–138, 1989.

de Silans, A. P., Monteny, B. A., and Lhomme, J. P.: The correction of soil heat flux measurements to derive an accurate surface energy balance by the Bowen ratio method, Journal of Hydrology, 188, 453–465, 1997.

Decharme, B., Boone, A., Delire, C., and Noilhan, J.: Local evaluation of the Interaction between Soil Biosphere Atmosphere soil multilayer

1080   diffusion scheme using four pedotransfer functions, Journal of Geophysical Research: Atmospheres, 116, 2011.

Delire, C., Séférian, R., Decharme, B., Alkama, R., Calvet, J.-C., Carrer, D., Gibelin, A.-L., Joetzjer, E., Morel, X., Rocher, M., et al.: The global land carbon cycle simulated with ISBA-CTRIP: Improvements over the last decade, Journal of Advances in Modeling Earth Systems, 12, e2019MS001 886, 2020.

Ding, R., Kang, S., Du, T., Hao, X., and Tong, L.: Modeling crop water use in an irrigated maize cropland using a biophysical process-based

1085   model, Journal of Hydrology, 529, 276–286, 2015.

Dong, J., Dirmeyer, P. A., Lei, F., Anderson, M. C., Holmes, T. R., Hain, C., and Crow, W. T.: Soil evaporation stress determines soil moisture-evapotranspiration coupling strength in land surface modeling, Geophysical Research Letters, 47, e2020GL090 391, 2020.

Duursma, R. A., Blackman, C. J., Lopéz, R., Martin-StPaul, N. K., Cochard, H., and Medlyn, B. E.: On the minimum leaf conductance: its role in models of plant water use, and ecological and environmental controls, New Phytologist, 221, 693–705, 2019.

1090 Feng, H., Wu, Z., Dong, J., Zhou, J., Brocca, L., and He, H.: Transpiration–Soil evaporation partitioning determines inter-model differences in soil moisture and evapotranspiration coupling, Remote Sensing of Environment, 298, 113 841, 2023.

Foken, T. and Napo, C. J.: Micrometeorology, vol. 2, Springer, 2008.

Gerke, H. H. and Van Genuchten, M. T.: A dual-porosity model for simulating the preferential movement of water and solutes in structured porous media, Water resources research, 29, 305–319, 1993.

1095 González-Armas, R., Vilà-Guerau de Arellano, J., Mangan, M. R., Hartogensis, O., and de Boer, H.: On the impact of canopy environmental variables on the diurnal dynamics of the leaf and canopy water and carbon dioxide exchange, EGUsphere, 2023, 1–31, 2023.

Goudriaan, J., Van Laar, H., Van Keulen, H., and Louwerse, W.: Photosynthesis, CO2 and plant production, in: Wheat growth and modelling, pp. 107–122, Springer, 1985.

Groh, J., Slawitsch, V., Herndl, M., Graf, A., Vereecken, H., and Pütz, T.: Determining dew and hoar frost formation for a low mountain range

1100   and alpine grassland site by weighable lysimeter, Journal of Hydrology, 563, 372–381, 2018a.

Groh, J., Stumpp, C., Lücke, A., Pütz, T., Vanderborght, J., and Vereecken, H.: Inverse estimation of soil hydraulic and transport parameters of layered soils from water stable isotope and lysimeter data, Vadose Zone Journal, 17, 1–19, 2018b.

Guo, L. and Lin, H.: Addressing two bottlenecks to advance the understanding of preferential flow in soils, Advances in agronomy, 147, 61–117, 2018.

1105 Harris, P. P., Folwell, S. S., Gallego-Elvira, B., Rodríguez, J., Milton, S., and Taylor, C. M.: An evaluation of modeled evaporation regimes in Europe using observed dry spell land surface temperature, Journal of Hydrometeorology, 18, 1453–1470, 2017.

He, C., Valayamkunnath, P., Barlage, M., Chen, F., Gochis, D., Cabell, R., Schneider, T., Rasmussen, R., Niu, G., Yang, Z., et al.: The community Noah-MP land surface modeling system technical description version 5.0, Tech. rep., NCAR Technical Note NCAR/TN-575+ STR, doi: 10.5065/ew8g-yr95, 2023.

1110 Hengl, T., Mendes de Jesus, J., Heuvelink, G. B., Ruiperez Gonzalez, M., Kilibarda, M., Blagotić, A., Shangguan, W., Wright, M. N., Geng, X., Bauer-Marschallinger, B., et al.: SoilGrids250m: Global gridded soil information based on machine learning, PLoS one, 12, e0169 748, 2017.

Iden, S. C., Blöcher, J. R., Diamantopoulos, E., and Durner, W.: Capillary, film, and vapor flow in transient bare soil evaporation (1): Identifiability analysis of hydraulic conductivity in the medium to dry moisture range, Water Resources Research, 57, e2020WR028 513,
1115 2021.

Ivanov, V. Y., Bras, R. L., and Vivoni, E. R.: Vegetation-hydrology dynamics in complex terrain of semiarid areas: 1. A mechanistic approach to modeling dynamic feedbacks, Water Resources Research, 44, 2008.

Jackisch, C., Germer, K., Graeff, T., Andrä, I., Schulz, K., Schiedung, M., Haller-Jans, J., Schneider, J., Jaquemotte, J., Helmer, P., et al.: Soil moisture and matric potential–an open field comparison of sensor systems, Earth System Science Data, 12, 683–697, 2020.

1120 Jacobs, C., Van den Hurk, B., and De Bruin, H.: Stomatal behaviour and photosynthetic rate of unstressed grapevines in semi-arid conditions, Agricultural and Forest Meteorology, 80, 111–134, 1996.

Jasinski, M. F., Borak, J., and Crago, R.: Bulk surface momentum parameters for satellite-derived vegetation fields, Agricultural and forest meteorology, 133, 55–68, 2005.

Jiang, Q., Zhang, J.-Y., Guo, X., Monteros, M. J., and Wang, Z.-Y.: Physiological characterization of transgenic alfalfa (Medicago sativa) plants
1125 for improved drought tolerance, International Journal of Plant Sciences, 170, 969–978, 2009.

Jiménez, C., Prigent, C., Mueller, B., Seneviratne, S. I., McCabe, M., Wood, E. F., Rossow, W. B., Balsamo, G., Betts, A., Dirmeyer, P., et al.: Global intercomparison of 12 land surface heat flux estimates, Journal of Geophysical Research: Atmospheres, 116, 2011.

Jiménez, M. A., Grau, A., Martínez-Villagrasa, D., and Cuxart, J.: Characterization of the marine-air intrusion Marinada in the eastern Ebro sub-basin, International Journal of Climatology, 43, 7682–7699, 2023.

1130 Jung, M., Reichstein, M., and Bondeau, A.: Towards global empirical upscaling of FLUXNET eddy covariance observations: validation of a model tree ensemble approach using a biosphere model, Biogeosciences, 6, 2001–2013, 2009.

Kerstiens, G.: Cuticular water permeability and its physiological significance, Journal of experimental botany, 47, 1813–1832, 1996.

Kohfahl, C., Saaltink, M. W., and Bermudo, F. R.: Vapor flow control in dune sediments under dry bare soil conditions, Science of The Total Environment, 786, 147 404, 2021.

1135 Krevh, V., Groh, J., Weihermüller, L., Filipović, L., Defterdarović, J., Kovač, Z., Magdić, I., Lazarević, B., Baumgartl, T., and Filipović, V.: Investigation of hillslope vineyard soil water dynamics using field measurements and numerical modeling, Water, 15, 820, 2023.

Lehmann, P., Merlin, O., Gentine, P., and Or, D.: Soil texture effects on surface resistance to bare-soil evaporation, Geophysical Research Letters, 45, 10–398, 2018.

Lohou, F., Kergoat, L., Guichard, F., Boone, A., Cappelaere, B., Cohard, J.-M., Demarty, J., Galle, S., Grippa, M., Peugeot, C., et al.: Surface
1140 response to rain events throughout the West African monsoon, Atmospheric Chemistry and Physics, 14, 3883–3898, 2014.

Lunel, T., Jimenez, M. A., Cuxart, J., Martinez-Villagrasa, D., Boone, A., and Le Moigne, P.: The marinada fall wind in the eastern Ebro sub-basin: physical mechanisms and role of the sea, orography and irrigation, Atmospheric Chemistry and Physics, 24, 7637–7666, 2024.

Ma, S., Eichelmann, E., Wolf, S., Rey-Sanchez, C., and Baldocchi, D. D.: Transpiration and evaporation in a Californian oak-grass savanna: Field measurements and partitioning model results, Agricultural and Forest Meteorology, 295, 108 204, 2020.

1145 MacBean, N., Scott, R. L., Biederman, J. A., Ottlé, C., Vuichard, N., Ducharne, A., Kolb, T., Dore, S., Litvak, M., and Moore, D. J.: Testing water fluxes and storage from two hydrology configurations within the ORCHIDEE land surface model across US semi-arid sites, Hydrology and Earth System Sciences, 24, 5203–5230, 2020.

Malik, W., Boote, K. J., Hoogenboom, G., Cavero, J., and Dechmi, F.: Adapting the CROPGRO model to simulate alfalfa growth and yield, Agronomy Journal, 110, 1777–1790, 2018.

1150 Mangan, M., Hartogensis, O., Branch, O., Martinez Villagrasa, D., Boone, A., Canut, G., Cuxart, J., de Boar, H., Le Page, M., Miro, J., Price, J., and Vila Guerau de Arellano, J.: LIAISE_UNIFIEDEC_WUR_10MIN_L1 [Dataset] Aeris, https://doi.org/10.25326/389, 2022.

Martí, B. and Boone, A.: Dry Surface Layer SURFEX simulations and necessary code (Versión 1), https://doi.org/10.5281/zenodo.15205476, 2025.

Martínez-Villagrasa, D., M., B., Cuxart, J., and Wrenger, B.: LIAISE_IRTA-CORN_UIB_SEB-10MIN_L2 [Dataset] Aeris,
1155 https://doi.org/10.25326/344, 2022.

Mauder, M., Foken, T., and Cuxart, J.: Surface-energy-balance closure over land: a review, Boundary-layer meteorology, 177, 395–426, 2020.

Merlin, O., Stefan, V. G., Amazirh, A., Chanzy, A., Ceschia, E., Er-Raki, S., Gentine, P., Tallec, T., Ezzahar, J., Bircher, S., et al.: Modeling soil evaporation efficiency in a range of soil and atmospheric conditions using a meta-analysis approach, Water Resources Research, 52, 3663–3684, 2016.

1160 Merz, S., Pohlmeier, A., Balcom, B. J., Enjilela, R., and Vereecken, H.: Drying of a natural soil under evaporative conditions: A comparison of different magnetic resonance methods, Applied magnetic resonance, 47, 121–138, 2016.

Milly, P.: A simulation analysis of thermal effects on evaporation from soil, Water Resources Research, 20, 1087–1098, 1984.

Miralles, D., De Jeu, R., Gash, J., Holmes, T., and Dolman, A.: Magnitude and variability of land evaporation and its components at the global scale, Hydrology and Earth System Sciences, 15, 967–981, 2011.

1165 Miró, J. R.: LIAISE_IRTA-ET0_SMC_SEB-10MN_L1 [Dataset] Aeris, https://liaise.aeris-data.fr/page-catalogue/?uuid=7f83e709-4ed4-49f1-b26f-c45d0519e4cf, 2021.

Mohamed, A. A.-R., WATANABE, K., and KUROKAW, U.: Simple method for determining the bare soil resistance to evaporation, Journal of Groundwater Hydrology, 39, 97–113, 1997.

Mouradi, M., Farissi, M., Lahrizi, Y., Oukaltouma, K., Saaidi, A., Khadraji, A., Bouizgaren, A., and Ghoulam, C.: Water deficit effects on
1170 canopy light interception, chlorophyll fluorescence, and stomatal conductance in Moroccan alfalfa genotypes, Plant Physiology Reports, 27, 469–480, 2022.

Napoly, A., Boone, A., Samuelsson, P., Gollvik, S., Martin, E., Seferian, R., Carrer, D., Decharme, B., and Jarlan, L.: The interactions between soil–biosphere–atmosphere (ISBA) land surface model multi-energy balance (MEB) option in SURFEXv8–Part 2: Introduction of a litter formulation and model evaluation for local-scale forest sites, Geoscientific Model Development, 10, 1621–1644, 2017.

1175 Nimmo, J. R., Wiekenkamp, I., Araki, R., Groh, J., Singh, N. K., Crompton, O., Wyatt, B. M., Ajami, H., Giménez, D., Hirmas, D. R., et al.: Identifying preferential flow from soil moisture time series: Review of methodologies, Vadose Zone Journal, 24, e70 017, 2025.

Niu, G.-Y., Yang, Z.-L., Mitchell, K. E., Chen, F., Ek, M. B., Barlage, M., Kumar, A., Manning, K., Niyogi, D., Rosero, E., et al.: The community Noah land surface model with multiparameterization options (Noah-MP): 1. Model description and evaluation with local-scale measurements, Journal of Geophysical Research: Atmospheres, 116, 2011.

1180 Noilhan, J. and Mahfouf, J.-F.: The ISBA land surface parameterisation scheme, Global and planetary Change, 13, 145–159, 1996.

Noilhan, J. and Planton, S.: A simple parameterization of land surface processes for meteorological models, Monthly weather review, 117, 536–549, 1989.

Oke, T. R.: Boundary layer climates, Routledge, 2002.

Or, D., Lehmann, P., Shahraeeni, E., and Shokri, N.: Advances in soil evaporation physics—A review, Vadose Zone Journal, 12, 1–16, 2013.

1185 Paulus, S. J., Orth, R., Lee, S.-C., Hildebrandt, A., Jung, M., Nelson, J. A., El-Madany, T. S., Carrara, A., Moreno, G., Mauder, M., et al.: Interpretability of negative latent heat fluxes from eddy covariance measurements in dry conditions, Biogeosciences, 21, 2051–2085, 2024.

Pérez-Anta, I., Rubio, E., López-Serrano, F. R., Garcés, D., Andrés-Abellán, M., Picazo, M., Chebbi, W., Arquero, R., and García-Morote, F. A.: Transpiration Dynamics of Esparto Grass (Macrochloa tenacissima (L.) Kunth) in a Semi-Arid Mediterranean Climate: Unraveling the Impacts of Pine Competition, Plants, 13, 661, 2024.

1190 Philip, J. and De Vries, D. d.: Moisture movement in porous materials under temperature gradients, Eos, Transactions American Geophysical Union, 38, 222–232, 1957.

Price, J.: LIAISE_ELS-PLANS_UKMO_MTO-30MIN$_{L2}[Dataset]Aeris$, https://doi.org/10.25326/430, 2023.

Ran, L., Pleim, J., Gilliam, R., Binkowski, F. S., Hogrefe, C., and Band, L.: Improved meteorology from an updated WRF/CMAQ modeling system with MODIS vegetation and albedo, Journal of Geophysical Research: Atmospheres, 121, 2393–2415, 2016.

Raoult, N., Delorme, B., Ottlé, C., Peylin, P., Bastrikov, V., Maugis, P., and Polcher, J.: Confronting soil moisture dynamics from the ORCHIDEE

1195 land surface model with the ESA-CCI product: Perspectives for data assimilation, Remote Sensing, 10, 1786, 2018.

Raoult, N., Ottlé, C., Peylin, P., Bastrikov, V., and Maugis, P.: Evaluating and optimizing surface soil moisture drydowns in the ORCHIDEE land surface model at in situ locations, Journal of Hydrometeorology, 22, 1025–1043, 2021.

Sakaguchi, K. and Zeng, X.: Effects of soil wetness, plant litter, and under-canopy atmospheric stability on ground evaporation in the Community Land Model (CLM3. 5), Journal of Geophysical Research: Atmospheres, 114, 2009.

1200 Schlesinger, W. H. and Jasechko, S.: Transpiration in the global water cycle, Agricultural and Forest Meteorology, 189, 115–117, 2014.

Schneider, J., Groh, J., Pütz, T., Helmig, R., Rothfuss, Y., Vereecken, H., and Vanderborght, J.: Prediction of soil evaporation measured with weighable lysimeters using the FAO Penman–Monteith method in combination with Richards' equation, Vadose Zone Journal, 20, e20 102, 2021.

Schübl, M., Brunetti, G., Fuchs, G., and Stumpp, C.: Estimating vadose zone water fluxes from soil water monitoring data: a comprehensive

1205 field study in Austria, Hydrology and Earth System Sciences, 27, 1431–1455, 2023.

Sellers, P., Mintz, Y., Sud, Y. e. a., and Dalcher, A.: A simple biosphere model (SiB) for use within general circulation models, Journal of the atmospheric sciences, 43, 505–531, 1986.

Sellers, P., Randall, D., Collatz, G., Berry, J., Field, C., Dazlich, D., Zhang, C., Collelo, G., and Bounoua, L.: A revised land surface parameterization (SiB2) for atmospheric GCMs. Part I: Model formulation, Journal of climate, 9, 676–705, 1996.

1210 Sellers, P. J., Hall, F. G., Asrar, G., Strebel, D., and Murphy, R.: An overview of the first international satellite land surface climatology project (ISLSCP) field experiment (FIFE), Journal of Geophysical Research: Atmospheres, 97, 18 345–18 371, 1992a.

Sellers, P. J., Heiser, M. D., and Hall, F. G.: Relations between surface conductance and spectral vegetation indices at intermediate (100 m2 to 15 km2) length scales, Journal of Geophysical Research: Atmospheres, 97, 19 033–19 059, 1992b.

Shokrana, M. S. B. and Ghane, E.: Measurement of soil water characteristic curve using HYPROP2, MethodsX, 7, 100 840, 2020.

1215 Simó, G., Martínez-Villagrasa, D., Jiménez, M. A., Caselles, V., and Cuxart, J.: Impact of the surface–atmosphere variables on the relation between air and land surface temperatures, Meteorology and Climatology of the Mediterranean and Black Seas, pp. 219–233, 2019.

Snyder, W. C., Wan, Z., Zhang, Y., and Feng, Y.-Z.: Classification-based emissivity for land surface temperature measurement from space, International Journal of Remote Sensing, 19, 2753–2774, 1998.

Sobaga, A., Decharme, B., Habets, F., Delire, C., Enjelvin, N., Redon, P.-O., Faure-Catteloin, P., and Le Moigne, P.: Assessment of the interactions between soil–biosphere–atmosphere (ISBA) land surface model soil hydrology, using four closed-form soil water relationships and several lysimeters, Hydrology and Earth System Sciences, 27, 2437–2461, 2023.

Swenson, S. and Lawrence, D.: Assessing a dry surface layer-based soil resistance parameterization for the Community Land Model using GRACE and FLUXNET-MTE data, Journal of Geophysical Research: Atmospheres, 119, 10–299, 2014.

Takata, K., Emori, S., and Watanabe, T.: Development of the minimal advanced treatments of surface interaction and runoff, Global and planetary Change, 38, 209–222, 2003.

Travis, R. and Reed, R.: The Solar Tracking Pattern in a Closed Alfalfa Canopy 1, Crop Science, 23, 664–668, 1983.

Van de Griend, A. A. and Owe, M.: Bare soil surface resistance to evaporation by vapor diffusion under semiarid conditions, Water Resources Research, 30, 181–188, 1994.

Van Diepen, K., Goudriaan, J., Vilà-Guerau de Arellano, J., and De Boer, H.: Comparison of C3 photosynthetic responses to light and CO2 predicted by the leaf photosynthesis models of Farquhar et al.(1980) and Goudriaan et al.(1985), Journal of Advances in Modeling Earth Systems, 14, e2021MS002 976, 2022.

Vereecken, H., Weihermüller, L., Assouline, S., Šimnek, J., Verhoef, A., Herbst, M., Archer, N., Mohanty, B., Montzka, C., Vanderborght, J., et al.: Infiltration from the pedon to global grid scales: An overview and outlook for land surface modeling, Vadose Zone Journal, 18, 1–53, 2019.

Von Caemmerer, S. v. and Farquhar, G. D.: Some relationships between the biochemistry of photosynthesis and the gas exchange of leaves, Planta, 153, 376–387, 1981.

Wang, L., Good, S. P., and Caylor, K. K.: Global synthesis of vegetation control on evapotranspiration partitioning, Geophysical Research Letters, 41, 6753–6757, 2014.

Wang, X.: Vapor flow resistance of dry soil layer to soil water evaporation in arid environment: An overview, Water, 7, 4552–4574, 2015.

Wang, Z., Zhan, C., Ning, L., and Guo, H.: Evaluation of global terrestrial evapotranspiration in CMIP6 models, Theoretical and Applied Climatology, 143, 521–531, 2021.

Way, D. A., Katul, G. G., Manzoni, S., and Vico, G.: Increasing water use efficiency along the C3 to C4 evolutionary pathway: a stomatal optimization perspective, Journal of Experimental Botany, 65, 3683–3693, 2014.

Weihermüller, L., Lehmann, P., Herbst, M., Rahmati, M., Verhoef, A., Or, D., Jacques, D., and Vereecken, H.: Choice of pedotransfer functions matters when simulating soil water balance fluxes, Journal of Advances in Modeling Earth Systems, 13, e2020MS002 404, 2021.

Xue, Y., Zeng, F. J., and Schlosser, C. A.: SSiB and its sensitivity to soil properties—A case study using HAPEX-Mobilhy data, Global and Planetary Change, 13, 183–194, 1996.

Yoo, C. Y., Pence, H. E., Hasegawa, P. M., and Mickelbart, M. V.: Regulation of transpiration to improve crop water use, Critical Reviews in Plant Science, 28, 410–431, 2009.

Yuan, Y., Wang, X., Yin, F., and Zhan, J.: Examination of the quantitative relationship between vegetation canopy height and LAI, Advances in Meteorology, 2013, 964 323, 2013.

Zhang, C., Li, L., and Lockington, D.: A physically based surface resistance model for evaporation from bare soils, Water Resources Research, 51, 1084–1111, 2015.

Zhang, C., Shi, S., Liu, Z., Yang, F., and Yin, G.: Drought tolerance in alfalfa (Medicago sativa L.) varieties is associated with enhanced
1255   antioxidative protection and declined lipid peroxidation, Journal of plant physiology, 232, 226–240, 2019.

Zhang, N. and Wang, Z.: Review of soil thermal conductivity and predictive models, International Journal of Thermal Sciences, 117, 172–183,
2017.